

Thermobarometric constraints on the Late Cretaceous tectonic and magmatic evolution of
the Coast Plutonic Complex, western British Columbia, Canada

David M. Pearson^{*}, Mihai N. Ducea^{*}, George E. Gehrels^{*}, Margaret E. Rusmore^{**}, Glenn
J. Woodsworth^{***}

Department of Geosciences, University of Arizona

^{*}Department of Geosciences, University of Arizona 1040 E. 4th St., Tucson, AZ, 85721,
United States. E-mail: pearsond@email.arizona.edu, Telephone: 520-621-6000, Fax:

520-621-2672.

^{**}Department of Geology, Occidental College, Los Angeles, California

^{***}Geological Survey of Canada, Vancouver, British Columbia, Canada

Abstract

New geothermobarometric (PT) results from the western metamorphic belt of the Coast Plutonic Complex of western British Columbia (BC) and southeastern Alaska (AK) confirm the presence of an inverted metamorphic gradient in Douglas Channel with equilibration pressures of metamorphic rocks increasing northeastward from ~5 kbar at Gil Island to ~9.5 kbar 2-3 km southwest of the Coast shear zone. PT results in Dean Channel and Mussel Inlet suggest that the crust is exposed to a shallower level than corresponding rocks >250 km north in Prince Rupert and southeastern AK. Most rocks are compatible with clockwise P-T-t paths, culminating in amphibolite and locally granulite facies peak metamorphic conditions (on average ~6-7 kbar, ~700°C), followed by steep exhumation paths in PT space. The most reasonable model to explain these results is one in which rocks are deformed by crustal thickening with additional thermal input from concurrent magmatism. An additional PT result in Mussel Inlet indicates P_s of ~10.7 kbar, >4 kbar higher than rocks 5 km to the west, compatible with transport to the mid crust during voluminous Late Cretaceous magmatism. U-Pb zircon results from this study are in accord with preliminary results from other workers in the region and indicate that Cretaceous deformation and magmatism lasted longer southeast of Prince Rupert than to the north. For rocks south of Prince Rupert and north of Bella Coola, final amalgamation of the Insular and Intermontane terranes against the western margin of North America likely outlasted the accretionary event farther north.

In the framework of the Coast Mountains as a continental magmatic arc, PT results from country rocks in this study indicate that, as expected, T_s in the mid crust

during magmatism are sufficient (locally in excess of 700°C) to cause widespread partial melting in the mid to lower crust. Previous isotopic studies of the Coast Mountains have demonstrated that most plutons in the region contain juvenile isotopic signatures with mixed mantle- and crustal-derived melts. Results from this study provide evidence that, in addition to isotopic contamination of mantle-derived melts during ascent through the crust, crustal melt contributions can be significant in continental magmatic arcs.

Introduction

The Coast Plutonic Complex of western British Columbia (BC) and southeastern Alaska (AK) is a composite magmatic arc of Jurassic through early Tertiary age (Figure 1). Virtually the entire length of the arc is cut by the Coast shear zone, a northwest-striking zone of ductile deformation that continues for >1200 km along the northwestern margin of North America (Rusmore et al., 2001). Previous studies in southeastern AK and northern BC have centered on understanding terrane accretion in time and space and documenting the structural histories of rocks on both sides of the Coast shear zone. Researchers have been successful in delineating the relative timing of structural and metamorphic events, but regional tectonic studies of the arc are complicated by its complex accretionary history and long record of superimposed magmatism and overprinting metamorphism. Some significant findings include: 1) South of Juneau, the Coast shear zone separates two different crustal panels, the Central Gneiss Complex on the northeast, and the western metamorphic belt on the southwest, each with differing temporal patterns of magmatism and each recording different conditions of metamorphism (Crawford and Hollister, 1982); 2) Research in southeastern AK and northern coastal BC in the western metamorphic belt has revealed an inverted metamorphic gradient with pressures increasing northeastward toward the Coast shear zone (Crawford and Hollister, 1982; Crawford et al., 1987); 3) Deformation southwest of the Coast shear zone likely resulted from mid Cretaceous crustal shortening related to final amalgamation of the Insular superterrane with the Intermontane superterrane and the ancestral margin of western North America (Monger et al., 1982); and 4) Major

exhumation of the Central Gneiss Complex, at least in the vicinity of Douglas Channel, was concurrent with movement along a northeast-dipping regional normal fault and was subsequent to documented motion along the Coast shear zone (Rusmore et al., 2005). Ongoing research aims to understand the Cretaceous-Tertiary history of the orogen, including the significance and history of the Coast shear zone and the continuation of plutonic and metamorphic rocks south of Prince Rupert.

The main purpose of this study is to elucidate the pressure-temperature-time (P-T-t) paths of some metasedimentary rocks of western BC south of Prince Rupert and north of Bella Coola to compliment work done by others to the north, to investigate along-strike regional variations in the arc southwest of the Coast shear zone, and to shed light on processes active in the mid-crust in continental magmatic arcs. Thermobarometric work constitutes the core of the project, with complimentary U-Pb zircon geochronology.

Geologic background

The western metamorphic belt of southeastern AK comprises the Proterozoic to Paleozoic continental margin rocks of Yukon-Tanana terrane (Gehrels et al., 1990) and Paleozoic to Mesozoic arc-derived rocks of Taku terrane (Gehrels, 2002). Correlative rocks of the western metamorphic belt of western BC have been called the Nisling Assemblage (Figure 1). Following a Devonian through Jurassic history of arc magmatism interpreted as resulting from the opening and closure of the Slide Mountain ocean adjacent to the margin of Laurentia, the Nisling Assemblage and associated rocks of the Intermontane terrane were amalgamated with the Insular terrane and accreted to the western margin of Laurentia in the mid-Jurassic (Colpron et al., 2007; Monger et al.,

1982). Marine basinal strata of the Gravina belt were deposited between the terranes in the Late Jurassic and Early Cretaceous (Berg et al., 1972), concurrent with arc magmatism in both the Insular terrane (Butler et al., 2006) and Intermontane terrane (Journey et al., 2000).

In the mid Cretaceous, the ocean basin closed and a ~1200 km arc-parallel west-vergent thrust system accommodated eastward underthrusting of the Insular terrane beneath the Intermontane terrane and western North America (Crawford and Hollister, 1982; Crawford et al., 1987; McClelland et al., 1992a; Rubin et al., 1990). Intermittent magmatism was superimposed on the terrane boundary and developing thrust belt with most U-Pb zircon age data recording cessation of thrust faulting near Prince Rupert and in southeastern Alaska by ~90 Ma (Klepeis et al., 1998; McClelland et al., 1992b; Sutter and Crawford, 1985). Contact metamorphism persisted from ~100-85 Ma as recorded by Sm-Nd garnet and U-Pb zircon age data (Stowell et al., 2001; Sutter and Crawford, 1985). Early Tertiary reverse and dextral transpressive (~65-55 Ma; Andronicos et al., 1999; Klepeis et al., 1998; Rusmore et al., 2005), and later, locally normal displacement on the Coast shear zone (~57-55 Ma; Klepeis et al., 1998) truncated metamorphic isograds formed during mid Cretaceous crustal thickening and contact metamorphism. The currently exposed metamorphic field gradient indicates a northeastward increase in equilibration P_s in the western metamorphic belt, with sub-greenschist facies rocks in the west grading across-strike to kyanite-bearing rocks that record P_s of up to 12 kbar adjacent to the southwestern boundary of the Coast shear zone (Crawford and Hollister, 1982; Crawford et al., 1987; Himmelberg and Brew, 2004; McClelland et al., 1991).

Although high T, locally granulite facies metamorphic conditions are preserved in the Central Gneiss Complex, relict kyanites have been found at several localities (Hollister, 1977; Klepeis et al., 1998; Stowell and Crawford, 2000), some of demonstrable mid to Late Cretaceous age (Rusmore et al., 2005). Metamorphism and exhumation of the western metamorphic belt had finished by the Late Cretaceous, whereas rocks of the Central Gneiss Complex continued to be metamorphosed at mid-crustal levels through the early Tertiary, followed by fast (1-2 mm/a), nearly isothermal exhumation from ~52-48 Ma accommodated on detachment faults bounding the eastern side of the Central Gneiss Complex (Andronicos et al., 2003; Hollister, 1982; Rusmore et al., 2005; van der Heyden, 1992).

In the context of work done in the western metamorphic belt of northern coastal BC and southeastern AK, most rocks collected for this study appear to be metamorphosed during regional mid-Cretaceous crustal thickening and concomitant magmatism. Few thermobarometric results have been published in western metamorphic belt rocks between Prince Rupert and Bella Coola, and published ages of metamorphism, magmatism, and deformation are sparse. In addition, significant changes in geology are visible on regional-scale maps near Bella Coola, particularly the lack of continuity of the Central Gneiss Complex and bounding detachment fault, and relatively higher amounts of Late Cretaceous to early Tertiary magmatism. The current study was motivated by some of these intriguing questions, in particular the large exposure of mid-crustal rocks that can yield insight into the construction of the largest batholith of the Phanerozoic.

Petrography and context of metamorphic rocks

For rocks used in thermobarometric calculations, we used a petrographic microscope to examine textural relationships among phases to carefully evaluate equilibrium/disequilibrium relationships and to better constrain metamorphic pressure-temperature-time (P-T-t) paths. Metamorphic rocks from this study are metasedimentary gneisses with predominantly pelitic, semipelitic, or volcanic protoliths. Equilibrium mineral assemblages, tabulated in Table 1, indicate that most samples experienced peak metamorphic conditions in the amphibolite to lower granulite facies. Reaction textures in some metamorphic rocks more tightly constrain P-T-t paths. The following are petrographic observations of studied samples from north to south.

Douglas Channel

Sample MT05127 is a metapelite collected on the south side of Douglas Channel ~3 km southwest of the Coast shear zone (Figure 2) that contains 3-4 mm garnet hypidioblasts with faint inclusion trails of quartz, biotite, and rare kyanite and staurolite. A well-developed matrix foliation is irregular and folded around garnets and poikiloblastic, up to 4 mm long, elongate tabs of kyanite. Muscovite is rare and usually occurs near biotite. Biotite is locally rimmed by chlorite.

Metamorphic rocks on the north side of Douglas Channel and west of the Coast shear zone are referred to as the Scotia-Quaal metamorphic belt, and were studied by Gareau (1991a, 1991b). Three samples from the Scotia-Quaal belt were collected for the purposes of this study. Sample GJP75, taken from about 2 km northeast of Kihess Creek, contains ~5 mm polygonal garnet porphyroclasts with aligned inclusion trails of flattened quartz, clinozoisite, and rare titanite. The foliation exhibited by garnet inclusions is

refolded into mm-scale crenulations that are absent from and discordant with the well-developed matrix foliation defined by abundant clinozoisite, lesser biotite, and rare, apparently stable muscovite (Figure 3a). Clinozoisite appears stable in the matrix, and chlorite has replaced many degraded biotite aggregates. Matrix quartz and clinozoisite are mostly $\sim 100\ \mu\text{m}$ in diameter. Larger quartz grains occur adjacent to garnet, however, and also in rare $\sim 1\ \text{mm}$ wide, discontinuous veins. Matrix biotite and muscovite are usually $\sim 200\text{-}400\ \mu\text{m}$ long; larger biotite ($\sim 1\ \text{mm}$ long) grains are present adjacent to garnet margins, locally associated with obliquely oriented muscovite. About $0.75\ \text{mm}$ long plagioclase crystals are splotchy and degraded, whereas smaller, $100\text{-}200\ \mu\text{m}$ long plagioclase grains are idioblastic.

GJP72 is from a locality $\sim 2\ \text{km}$ northeast of Gertrude Point in Douglas Channel and contains $5\text{-}10\ \text{mm}$ hornblende porphyroblasts with irregular margins and abundant inclusions that define an earlier, folded foliation. Garnet xenoblasts up to $4\ \text{mm}$ in diameter have embayed margins and contain inclusions of quartz and ilmenite. Muscovite and biotite define a moderately developed, irregular foliation, and locally contain rims or intergrowths of obliquely oriented chlorite grains.

Sample GJP70 is from a small pendant of metamorphosed volcanoclastic sandstones and breccias within the Ecstall pluton $\sim 3.5\ \text{km}$ north of Kiskosh Inlet. Garnet xenoblasts, mostly oval or lath-shaped and up to $7\ \text{mm}$ long, contain abundant quartz and rare chlorite inclusions, overall defining a foliation concordant with the long axes of garnet grains. Matrix grains are generally less than $50\ \mu\text{m}$ in diameter, with the exception of $\sim 2\text{-}4\ \text{mm}$, locally recrystallized muscovite porphyroblasts. Muscovite is

also present in garnet fractures roughly perpendicular to inclusion trails and long axes of garnet grains. A weak matrix foliation is defined mainly by biotite and garnet, but biotite is often oriented obliquely to the foliation. One garnet, originally round with many more inclusions in its core than in its rim, has one side broken off.

Gil Island

Sample GJP66 was collected from the northern end of Gil Island in a small cove south of Juan Point, ~1.5 m from a 1 m wide granitoid dike, and contains splotchy, originally cm-scale garnets. A moderately developed foliation defined by hornblende is folded around plagioclase, biotite, and ilmenite coronas at highly embayed garnet margins; in some places, little garnet remains. In one thin section, three epidote grains were found; two occur adjacent to or included in biotite and one is a splotchy grain in the matrix. Rare chlorite is present within or around biotite rims.

Sample GJP59 was collected at Fawcett Point, on the southern end of Gil Island (Figure 2), and contains 5-7 mm hypidioblastic garnets with inclusions of quartz and fractures roughly perpendicular to the matrix foliation. Matrix grains are relatively small ($\leq 100\text{-}200\ \mu\text{m}$) and quartz appears recrystallized, except for within pressure shadows adjacent to garnet. Some biotite is chloritized.

Mussel Inlet

Samples GJP48, GJP49, and MT05100 were all collected from the same locality in Mussel Inlet (Figure 4) and contain sillimanite pseudomorphs, commonly present as crystallographically-oriented prisms, that apparently replaced kyanite (Figure 3b). Biotite crystals are intergrown with needly or fibrous sillimanite. They mostly appear in

equilibrium, but locally sillimanite needles appear to replace biotite rims (Figure 3c). Rare muscovite appears unstable, is intergrown with biotite and sillimanite, and usually crosscuts the moderately developed foliation defined by biotite and mats of fibrolitic sillimanite. Very rare chlorite also rims some biotite grains and appears in some cracks within ≤ 1 cm diameter, inclusion-free, idioblastic to hypidioblastic garnets. Some quartz veins ~ 1.5 mm wide are also present, roughly parallel to the foliation.

Sample 06DP07, a garnet amphibolite gneiss from a locality about 1 km northeast, contains a hypidioblastic garnet ~ 6 mm in diameter, with inclusions of staurolite, hornblende, plagioclase, very splotchy muscovite and possible chlorite (Figure 3d). Rare biotite porphyroblasts are also present in the matrix, with locally chloritized rims.

Approximately 3 km along strike to the northwest of 06DP07, sample 06DP05 is a metapelite with hypidioblastic garnets ~ 2 -3 mm in diameter. Garnets are mostly inclusion-free but contain rare quartz and biotite. Muscovite is sparse and appears unstable, intergrown with biotite or sillimanite. Rare chlorite is present in some garnet fractures.

Sample GJP47, collected about 4 km across strike to the northeast, is a garnet-biotite amphibolite, with ~ 2 mm locally recrystallized plagioclase xenoblasts. Garnets are ~ 2 -3 mm in diameter, with embayed margins and abundant quartz and rare biotite, hornblende, and pyrite inclusions. Some biotite grains have thin chlorite rims.

Collected from ~ 100 -200 m from the GJP47 sample locality, 06WV16 exhibits a strong, irregular, folded foliation defined by biotite, sillimanite, and muscovite. Garnets

are hypidio- to idioblastic and contain rare small quartz, biotite, and muscovite inclusions. Quartz displays highly undulatory extinction and in some areas its rims are partially or completely recrystallized. Some large plagioclase (up to 5 mm) grains have bent twins, are partially degraded, and some are recrystallized. Muscovite is usually intergrown with biotite or sillimanite, but it is difficult to tell whether muscovite was stable during peak metamorphism.

Nearly along strike of GJP47, samples GJP45 and GJP46 are Al_2SiO_5 -absent metapelites with 1-1.5 mm hypidioblastic garnets. Mostly quartz with some ilmenite, garnet inclusions form curved trails, discordant to a moderately developed matrix foliation defined by biotite. Biotite also grew in some garnet fractures and, in the matrix, some biotite rims have been chloritized. Matrix quartz appears recrystallized, but feldspar does not.

06WV12, 06DP02 and 06DP01, from about 1 km across strike to the northeast, were collected from a locally migmatized metapelitic unit adjacent to its gradational northeastern contact with a tonalitic sill (sample 06DP03). Garnets contain mostly quartz and biotite inclusions with rare hornblende and rims are highly resorbed, with plagioclase coronas developed locally. Microcline is abundant in these rocks, often has inclusion-rich cores surrounded by inclusion-free rims, and twinning appears bent and extinction undulatory. In these rocks, matrix feldspar has not recrystallized, but quartz has.

Samples 06WV14 and 06WV15 were collected adjacent to the same contact as above, but across Mussel Inlet. Both samples are garnet-biotite amphibolites with granoblastic texture and ~4 mm garnet hypidioblasts with quartz inclusions. In 06WV15,

some plagioclase has visible zoning and is usually ~1 mm, whereas quartz is mostly ~200 μm . Some chlorite is present locally, usually on biotite rims, and epidote rarely appears adjacent to it.

Dean Channel

Sample GJP28 was collected from a metamorphic screen within the Ecstall Pluton equivalent exposed on the north side of Dean Channel ~3 km north of Farquhar River (Figure 5). The rock contains abundant amphibole with pleochroic green tschermakite cores and colorless cummingtonite (Papike, 1987) rims (Figure 3e). Large (up to ~1 cm in diameter), idioblastic garnets contain inclusion trails of plagioclase, tschermakite, and ilmenite, concordant to the well-developed matrix foliation.

Analytical methods

U-Pb zircon geochronology

U-Pb zircon geochronology was applied to three samples from this study to better constrain ages of magmatism, metamorphism, and deformation. All separations and analyses were performed at the University of Arizona. More detailed descriptions of separation and analysis procedures than those that follow are given in Gehrels et al. (2006).

Zircon grains from each sample were separated from their host rocks and mounted in epoxy, followed by ablation of 25–35 μm diameter by ~15 μm deep pits with a New Wave DUV193 Excimer laser (operating at a wavelength of 193 nm). Ablated material was subsequently transported by a carrier gas through the plasma torch of a Micromass *Isoprobe* multicollector inductively coupled plasma mass spectrometer (MC-ICPMS) and

U, Th, and Pb were all measured simultaneously in static mode. Each analysis consisted of one 20-s integration on peaks with the laser off (for backgrounds), 20 1-s integrations with the laser firing, and a 30-s delay to purge the previous sample and prepare for the next analysis.

Common Pb corrections were made using measured ^{204}Pb and assuming an initial Pb composition according to that predicted by Stacey and Kramers (1975); conservative uncertainties are 1.0 for $^{206}\text{Pb}/^{204}\text{Pb}$ and 0.3 for $^{207}\text{Pb}/^{204}\text{Pb}$. The effects of small amounts of ^{204}Hg present in the carrier gas on measurements of ^{204}Pb were minimized by subtracting ^{204}Hg and ^{204}Pb backgrounds during analyses.

Inter-element fractionation of Pb and U is generally 20%, whereas fractionation of Pb isotopes is generally ~3%. Routine analyses of a zircon standard of known age (generally every fifth measurement) were used to correct for this fractionation, generally resulting in uncertainties of 2–3% (2σ) for both $^{206}\text{Pb}/^{238}\text{U}$ and $^{206}\text{Pb}/^{207}\text{Pb}$ ages.

Measurement errors of $^{206}\text{Pb}/^{238}\text{U}$, $^{206}\text{Pb}/^{204}\text{Pb}$, and $^{206}\text{Pb}/^{207}\text{Pb}$ normally result in 1–2% (2σ) uncertainties in the $^{206}\text{Pb}/^{238}\text{U}$ and $^{206}\text{Pb}/^{207}\text{Pb}$ ages for samples >1.0 Ga. Because of the low signal intensity of ^{207}Pb for young samples like those from this study, however, $^{206}\text{Pb}/^{207}\text{Pb}$ age uncertainties are substantially larger than the 1–2% approximation for $^{206}\text{Pb}/^{238}\text{U}$ ages.

Analytical data are reported in Table 2. Uncertainties shown in these tables are at the 1σ level, and include only measurement errors.

In addition to analytical uncertainties described above, age uncertainties of magmatic and metamorphic zircon also arise from datasets complicated by older

inherited zircon, lead loss, or new zircon growth. The preferred interpretation of the concordia plot (Ludwig, 2001) for sample 06DP09, for example, is that several older Paleozoic zircon analyses represent isotopic inheritance from the source or host rock and that the younger, Cretaceous age cluster actually represents the crystallization age (Figure 6b). Similarly, core and rim zircon analyses from orthogneiss sample 06MR15 indicate that an older, Devonian crystallization age was isotopically perturbed in the Late Cretaceous/Early Tertiary (Figure 6c). To minimize errors resulting from inclusion of inappropriate analytical data in age calculations, we report weighted means (Ludwig, 2001) of concordant and overlapping $^{206}\text{Pb}/^{238}\text{U}$ analyses, with final uncertainties that include all random and systematic errors. All final ages are reported with 2σ uncertainties.

Geothermobarometry

Rocks with appropriate mineral assemblages were analyzed for equilibration P_s and T_s to evaluate conditions of metamorphism throughout the study area. Electron microprobe analyses were performed in the Lunar and Planetary Laboratory at the University of Arizona using a Cameca SX50 electron microprobe equipped with 4 LiF, PET, and TAP spectrometers. Counting times were 20 s with a 10 s background, an accelerating potential of 15 kV, and a beam current of 10-20 nA.

In addition to petrographic observations described in the previous section, we carefully evaluated inter- and intra-granular compositional variations of phases used in thermobarometric calculations with the electron microprobe to assess the attainment/maintenance of equilibrium in samples. Representative mineral compositions

used for thermobarometry are given in Table 3. Most samples from this study contain equilibrated garnet with nearly flat diffusion profiles and retrograde zoning at the rims (Figure 7). Some samples, however, preserve apparent growth zoning or non-retrograde perturbation to equilibrated garnet profiles, as indicated by slightly bell-shaped Mn profiles. For samples with flat garnet profiles, representative core analyses were used for thermobarometric calculations; for growth-zoned garnets, we used analyses near the garnet rims, adjacent to retrograde diffusion zoning. It is likely that growth zoning originally extended to garnet rims. Therefore, thermobarometric calculations using growth-zoned garnet analyses inside of retrograde zoning will underestimate peak metamorphic conditions.

Within all thin sections, minerals other than garnet that were used in thermobarometric calculations were analyzed both away from and adjacent to garnet rims to assess inter- and intragranular compositional variations. Variations in magnesium numbers ($Mg\# = MgO/(MgO+FeO)$) within individual biotite grains and among biotites near and away from garnet rims were generally less than 0.01, although matrix biotites of most samples have slightly higher $Mg\#s$ (<0.01) than other biotites adjacent to garnet rims in the same thin section. To minimize effects on PT calculations of retrograde diffusive exchange with garnet in all samples, only representative matrix biotite analyses away from garnet rims were used for thermometry.

Most samples also contain insignificant compositional variation in matrix plagioclase, with typical core-rim variations of $<An_1$. Matrix plagioclases in samples GJP72 and MT05127 however, display reverse zoning, with core-rim compositions of

An₆₅-An₆₀ and An₃₈-An₃₄, respectively. Compositional zoning in plagioclase adjacent to garnet rims is a bit more variable than matrix plagioclase, but most samples still contain rim plagioclase with <An₁ core-rim variation. Plagioclases adjacent to garnet that exhibit significant core-rim variation always have lower anorthite contents at their rims compared to in their cores. Samples GJP28 and MT05127 have core-rim plagioclase compositions of An₆₈-An₅₉ and An₄₂-An₃₂, respectively. Representative matrix plagioclase rim analyses were used for barometric calculations in all samples, based on the principle that minimal retrograde diffusion will have affected slowly diffusing matrix plagioclase rims. For amphibole, muscovite, K-feldspar, ilmenite, and rutile analyses, representative matrix core compositions were used.

For thermobarometric calculations with appropriate assemblages, we used formulations of the garnet-biotite thermometer (GarB) and garnet-aluminosilicate-quartz-plagioclase (GASP) barometer of Ganguly and Cheng (unpublished computer program, pers. comm., 2006). The formulations use the thermodynamic data of Berman (1988) and the experimental data for the pure end-member GASP reaction of Koziol and Newton (1988). The solution models used are those of Ganguly et al. (1996), Elkins and Grove (1990), and Douce et al. (1993), for garnet, plagioclase, and biotite, respectively. For calculations using the Ganguly and Cheng thermobarometric formulations, the percentage of Fe³⁺ in garnet was assumed to be 3% of the total percent Fe, and Fe³⁺ was assumed to be 11.6% of the total percent of Fe in biotite, based on average values for metapelites estimated by Holdaway (2000).

We also calculated pressures and temperatures of samples with the proper assemblages using the computer program THERMOCALC (Powell and Holland, 1988) version 3.25, which uses the internally consistent dataset HP98 (Holland and Powell, 1998), updated in 2003. The accompanying program, A-X, was used to calculate mineral formulae and activities. Among the advantages of using an internally consistent thermodynamic dataset to calculate equilibration pressures and temperatures is the ability to directly compare results using different mineral pairs and rock compositions. No water activities were assumed for THERMOCALC calculations.

For samples containing amphibole and no aluminosilicate, in addition to using THERMOCALC, calculations were performed using formulations of the garnet-amphibole-plagioclase barometer (GAP) and garnet-amphibole thermometer (GA) of Kohn and Spear (1990) and Graham and Powell (1984), respectively. Conservative errors of ± 0.5 kbar and $\pm 50^\circ\text{C}$ are reported for all GASP, GAP, GarB and GA calculations.

On average, THERMOCALC Ps are 0.6 kbar higher and Ts are $\sim 20^\circ\text{C}$ lower than Ps calculated with Ganguly and Cheng's GASP and GarB formulations (Table 4). THERMOCALC results are consistently higher than Graham and Powell's (1984) GAP barometer and Kohn and Spear's (1990) GA thermometer by ~ 3 kbar and $\sim 35^\circ\text{C}$, respectively.

Overall, there is good agreement among mean PT results of THERMOCALC (Powell and Holland, 1988) and PT points calculated with Ganguly and Cheng's GASP and GarB formulations. Both methods have their limitations; THERMOCALC produces

large error ellipses generated through propagation of component activity and analytical uncertainties, while Ganguly and Cheng's formulation is limited to aluminosilicate-bearing metapelitic assemblages. Because of the relative consistency in the calculations, however, mean PTs of THERMOCALC are considered good representations of equilibration Ps and Ts, and since not all rocks in this study contain proper assemblages for Ganguly and Cheng's preferred formulations, we refer to mean PT results calculated with THERMOCALC in our following discussions.

Results

U-Pb zircon geochronology and context

U-Pb zircon geochronology was applied to two rocks collected from Mussel Inlet and one rock from James Bay (Figures 1 and 4). Concordia plots and mean ages are given in Figure 6. Rocks dated from Mussel Inlet consist of a granodioritic orthogneiss that occurs in the north-central region (06MR15) and a sill-shaped tonalitic orthogneiss that crops out near the eastern edge of the inlet (06DP03). The granodioritic orthogneiss is mostly fine-grained and contains hornblende, biotite, rare garnet and epidote, and muscovite porphyroblasts within fractures that are approximately perpendicular to foliation. From a distance, the rock appears pale gray and massive, but a well-developed foliation defined by relatively sparse hornblende and biotite is apparent upon closer examination. U-Pb zircon results from the sample appear to be complicated by younger metamorphic zircon overgrowths or Pb loss from zircon rims too thin to be analyzed with the 25 μm laser spot. However, the clear, euhedral morphologies of retrieved zircons and the distribution of core vs. rim ages apparent from an average age plot (Figure 6c)

support the interpretation that a Middle to Late Devonian age of 397.1 ± 8.7 Ma is a good approximation to the crystallization age of the plutonic protolith.

In contrast, 06DP03 is a fine- to medium-grained tonalitic orthogneiss that contains hornblende, biotite, epidote, and titanite and exhibits a supersolidus deformation fabric. Near its gradational southwestern contact with a metapelitic unit described above (samples 06WV12, 06DP01 and 06DP02), the orthogneiss contains 1-2 cm garnets and is isoclinally folded. 64 of 69 zircon analyses from the sample are apparently concordant and yield a well-defined age of 85.7 ± 1.8 Ma that we interpret as the crystallization age (Figure 6a).

Other recent ongoing geochronologic studies in western BC have resulted in many yet unpublished U-Pb zircon and titanite ages, including several from Mussel Inlet and elsewhere that are pertinent to this study (G. Gehrels, pers. comm., 2006). Relevant ages are shown in Figure 4. Overall, results from this study and unpublished U-Pb zircon results from three sample localities in Mussel Inlet (G. Gehrels, pers. comm., 2006) indicate that tonalitic magmatism in Mussel Inlet was ongoing from ~ 93 Ma to ~ 83 Ma and that deformation persisted from at least ~ 86 Ma to ~ 83 Ma.

An additional sample analyzed during this study was collected from the south shore of James Bay in North Mathieson Channel (06DP09). The fine- to medium-grained granodiorite yielded an interpreted crystallization age of 85.9 ± 1.8 Ma, with several analyses clearly affected by inheritance of Paleozoic zircon (Figure 6a). This unit may correspond to another unpublished U-Pb zircon age of ~ 85 Ma obtained by G. Gehrels

(pers. comm., 2006) from a similar rock collected from the east side of Mathieson Channel.

Geothermobarometry

Consistent with petrographic observations, all samples from this study for which equilibration P_s and T_s were calculated record peak PT conditions in the amphibolite and lower granulite facies. A summary of thermobarometric results is given in Table 4 and results are shown graphically in Figure 8.

Discussion

Consistent with the inverted metamorphic gradient near Prince Rupert and northward, rocks within Douglas Channel record an increase in pressure northeastward toward the Coast shear zone, from ~5 kbar on Gil Island (GJP59) to ~9.5 kbar about 3 km southwest of the Coast shear zone (MT05127; Figure 2). Also, rocks to the north were apparently buried to deeper crustal levels than rocks to the southeast. Most rocks in Mussel Inlet, ~25 km southwest of the Coast shear zone and ~100 km southeast of Douglas Channel, record P_s of ~6.5 kbar (Figure 4). GJP70, however, which is ~25 km southwest of the Coast shear zone in Douglas Channel, records a P of 7.3 kbar. Similarly, one PT result from Douglas Channel, sample GJP72, which is ~12 km southwest of the Coast shear zone, records a P of 8.5 kbar (Figure 5), whereas ~175 km south in Dean Channel, ~13 km southwest of the Coast shear zone, GJP28 records a P of 5.7 kbar (Figure 5).

The presence of staurolite as inclusions in garnet and its absence in the matrix, and the occurrence of kyanite in garnet and in the matrix show that MT05127 followed a

clockwise prograde PT path to its peak metamorphic conditions of ~9.5 kbar and ~665°C (Spear and Cheney, 1989). As expected by equivalence with rocks to the north, this PT path is commonly attributed to crustal thickening by thrust faulting, although simple thermal modeling of a rock recording peak PT conditions experienced by MT05127 indicates that an elevated geotherm is also required (Thompson and England, 1984). The exhumation path of MT05127 is more difficult to ascertain, but the lack of staurolite and minimal chlorite on biotite rims are compatible with a steep decompression path (Spear and Cheney, 1989). Although the rock passed through the sillimanite field, the decompression rate may have been too fast relative to the rate of the kyanite-sillimanite transition at the PT conditions experienced by the rock during exhumation.

Samples west of MT05127 in Douglas Channel exhibit crenulations defined by garnet inclusions and testify to a protracted deformation history for these rocks. Moreover, though these rocks underwent peak metamorphism in the amphibolite facies at depths of ~20-25 km (~7.3-8.5+ kbar), some were overprinted by a later greenschist to amphibolite facies metamorphism, probably related to the intrusion of mid to Late Cretaceous or younger plutons.

South of Douglas Channel in Mussel Inlet, rocks preserve evidence of similar PT paths. Several workers have extensively described Al-rich garnet amphibolites containing staurolite (Arnold et al., 2000; Faryad and Hoinkes, 2006; Grew and Sandiford, 1985; Selverstone et al., 1984). While it appears that staurolite can be stable in Al-rich amphibolites over a wide range of pressures (~4-10 kbar, Arnold et al., 2000), the presence of staurolite, plagioclase, muscovite, and possible chlorite inclusions and the

lack of cordierite in garnet in 06DP07 indicate that this rock passed from high to low pressures during exhumation, probably along a steep PT path to avoid the growth of clinozoisite and staurolite in the matrix (Faryad and Hoinkes, 2006; Grew and Sandiford, 1985). An alternative but unlikely scenario is that following garnet growth and incorporation of inclusions, the rock was metasomatized to a more mafic composition.

Four samples collected near the western edge of Mussel Inlet (Figure 4) record consistent PTs of ~6.5 kbar and ~725°C, corresponding to metamorphism at mid-crustal depths of ~17-18 km. Results for three different samples collected from the same locality (GJP48, GJP49, MT05100) are shown to demonstrate the reproducibility of the PT estimates. Metamorphic reactions forming prismatic and fibrolitic sillimanite pseudomorphs in these rocks went to completion and did not preserve relict porphyroblasts. However, given that the pseudomorphs are commonly crystallographically-oriented indicates that these probably nucleated from another aluminosilicate. Sillimanite pseudomorphs after kyanite have been found in several other localities in the western Canadian Cordillera (e.g., Klepeis et al., 1998; McClelland et al., 1991; Norlander et al., 2002; Rusmore et al., 2005) and, considering the proximity of these rocks to others that can be linked to steep exhumation paths in PT space, the simplest explanation is that these rocks passed from the kyanite stability field into the sillimanite field at high T.

High Ps (~10.5 kbar) calculated for GJP47 in the north-central portion of Mussel Inlet are ~4 kbar higher than Ps calculated for rocks <5 km across strike to the southwest and indicate that this rock was metamorphosed at deeper crustal levels. Petrographic and

microprobe analyses of this rock show that, besides resorption of garnet rims, minerals in the rock appear equilibrated, stable, and relatively uniform in composition. It is unlikely that all other rocks for which PTs were calculated in Mussel Inlet represent reequilibrated assemblages that share a deep crustal metamorphic history with this rock, or that this rock retains a relict assemblage while other rocks in Mussel Inlet do not. A more reasonable hypothesis is that the rock was transported to the mid crust, possibly by a magmatic process, and emplaced along with mid-Cretaceous tonalitic sills. The process may be common in magmatic arcs where a high rate of magmatism leads to significantly elevated crustal temperatures ($>700^{\circ}\text{C}$) and possible intracrustal convection (Babeyko et al., 2002). An alternative, but more unlikely scenario is that the rock was displaced by a mid-Cretaceous thrust fault that was obscured by concurrent or later magmatism.

About 75 km south of Mussel Inlet in Dean Channel, petrographic observations and PT results indicate that sample GJP28 was metamorphosed in the amphibolite facies field at a slightly higher T than the epidote-out reaction (Spear, 1995). Furthermore, large ($\sim 500\ \mu\text{m}$) retrograde diffusion-zoned rims in idioblastic garnet, the absence of clinopyroxene and epidote, and the replacement of tschermakite by cummingtonite, likely via the rxn $\text{tschermakite} + \text{quartz} = \text{cummingtonite} + \text{plagioclase}$, suggest that this rock followed a steep (but relatively slow) exhumation path in PT space (Cooper and Lovering, 1970; Ouzegane et al., 2001; Spear, 1995).

Garnet inclusion trails discordant to matrix foliations, rare preservation of crenulation cleavages within garnet inclusion trails, meso-scale fold transposition, matrix foliations displaced by garnet porphyroblast margins, and grain size relationships of

quartz and feldspar all suggest that these rocks have a polydeformational history and that deformation accompanied and outlasted metamorphism. U-Pb zircon results from this study and unpublished results from other ongoing studies (G. Gehrels, pers. comm., 2006) demonstrate that deformation (and magmatism) was ongoing from ~86 Ma to <83 Ma. Other preliminary results from south of Mussel Inlet are in accordance with these observations and indicate that deformation and magmatism continued until ~75 Ma (Rusmore et al., 2006). These results are in contrast to Cretaceous deformation north of Prince Rupert which ended prior to ~90 Ma (Klepeis et al., 1998; McClelland et al., 1992b; Sutter and Crawford, 1985), although a general lack of post-90 Ma plutons may preclude the dating of younger deformation in the region. While more high T ages on metamorphic minerals are needed (e.g., garnet) to constrain regional metamorphic age patterns, these results suggest that in the south near Bella Coola, consistent with the regional U-Pb zircon data (Butler et al., 2002; Gehrels and Boghossian, 2000), final mid-Cretaceous amalgamation of the Insular terrane with the Intermontane terrane and western North America outlasted the accretionary event in Prince Rupert and northward. This along-strike change may also be related to the southern discontinuation of the Central Gneiss Complex and east-side detachment fault and the relatively shallower exposure of mid to Late Cretaceous plutons, but more work is needed.

Three non-mutually exclusive scenarios may explain the occurrence of shallower crustal levels in the south than those the same distance from the Coast shear zone to the north: 1) Relative displacement accommodated by the Coast shear zone varied significantly along strike; 2) Crustal thickening to the north was significantly greater than

that to the south and therefore less post-orogenic isostatic rebound precluded deeper rocks from being exhumed near Bella Coola; or 3) A divergence exists among the Coast shear zone and faults of the mid-Cretaceous thrust belt, so that the post- mid-Cretaceous Coast shear zone obliquely cut the thickened magmatic arc and subsequent displacement resulted in structurally correlative rocks exposed to different metamorphic depths. Resolution of the mechanism to explain the discrepancy is beyond the scope of this paper, although existing metamorphic, geochronologic, and structural data (Crawford and Hollister, 1982; Crawford et al., 1987; Hollister, 1982; Klepeis et al., 1998; McClelland et al., 1992a; McClelland et al., 1992b; Rubin et al., 1990; Rusmore et al., 2001; Rusmore et al., 2005) suggest that scenario 3) may be the most reasonable.

Aside from regional tectonics, PT results obtained for metasedimentary rocks near plutons of the Coast Plutonic Complex in western BC can improve our understanding of high T processes (e.g., melting, convection) taking place in the mid to lower crust in magmatic arcs. Equilibration Ts of all rocks were high (637-760°C), averaging ~710°C. Nearly all calculated PTs lie to the right of the wet granite solidus in PT space (Figure 8), and many rocks contain metamorphic K-feldspar. While evidence for partial melting is not present in all of these rocks, the common occurrence of graphite in metapelites significantly decreases water activities and depresses the K-feldspar dehydration reaction to lower Ts, indicating that even if thermometric estimates for the rocks are high, most of these rocks have undergone at least some degree of partial melting. Even more significant is relatively higher Ts that would be expected in the lower crust.

Another interesting result of this study is that despite high Ts calculated for rocks in Mussel Inlet, almost completely inherited, euhedral zircons were preserved in the Devonian orthogneiss that crops out in Mussel Inlet. If magmatic/metamorphic fluids infiltrated country rocks into which ~80 Ma plutons were intruded in Mussel Inlet, then they may have been saturated with respect to zircon (Hanchar and Watson, 2003; Miller et al., 2003). Alternatively, although zircon was subjected to the Ps and Ts of the surrounding country rock, it remained stable or metastable because it did not come into contact with a melt or fluid phase (Miller et al., 2003).

Conclusions

New PT results from this study confirm the presence of an inverted metamorphic gradient in Douglas Channel and suggest that shallower crustal levels are exposed south of Prince Rupert. Most rocks are compatible with clockwise PT paths, culminating in amphibolite to lower granulite facies peak metamorphic conditions (~6-7 kbar, ~710°C), followed by steep exhumation paths in PT space. A model in which rocks are deformed by crustal thickening with additional thermal input from concurrent magmatism is the most reasonable. One rock in Mussel Inlet preserves a peak pressure of ~10.7 kbar, >4 kbar higher than rocks 5 km to the west. The rock may have been transported to the mid crust along with plutonic sills in the area during ongoing magmatism in the mid Cretaceous, possible evidence for intracrustal convective overturn produced in models of the Andes to account for high heat flow in active magmatic arcs (Babeyko et al., 2002).

U-Pb zircon results from this study are in accord with preliminary results from other workers in the region (e.g, G. Gehrels, pers. comm., 2006; Rusmore et al., 2006)

and indicate that Cretaceous deformation and magmatism may have lasted longer south of Prince Rupert than to the north. This suggests that final amalgamation of the Insular and Intermontane terranes against the western margin of North America outlasted the accretionary event in the north. This along-strike change may be related to the southern discontinuation of the Central Gneiss Complex and east-side detachment fault, and the observation that shallower crustal levels are exposed in the western metamorphic belt near latitude 52° N, but more work is needed.

In the framework of the Coast Mountains as a continental magmatic arc, results from country rocks in this study indicate that, as expected, Ts in the mid crust during magmatism (~710°C) are sufficient to cause widespread partial melting in the crust. Previous Nd isotopic studies of the Coast Mountains have demonstrated that most plutons in the region contain juvenile isotopic signatures with mixed mantle- and crustal-derived melts (Patchett et al., 1998). Isotopic studies have difficulty, however, distinguishing crustally contaminated mantle-derived melts ascending through the lower and mid crust from mingling of mantle and crustal melt sources. Results from this study provide evidence for other models (e.g., Hollister and Andronicos, 2006) suggesting that ongoing magmatism in continental magmatic arcs can significantly heat the crust and increase contributions of crustal melts.

Acknowledgements

This research was supported by NSF grants EAR-0309885 (MD) and EAR-0310011 (MR), and EAR-0443387 (GG) NSF support of the Arizona LaserChron Center at the UA. DP acknowledges research support from ChevronTexaco, ExxonMobil, and a

Galileo Circle scholarship from the UA College of Science. Paul Wetmore and Jon Patchett assisted with sample collection in 2004, Ken Domanik and Mark Baker provided invaluable instrument assistance, Victor Valencia and Alex Pullen helped with zircon sample preparation, Gelu Costin and Ned Brown helped with petrography, and Alex Robinson and undergrads Jared Hamilton and Shannon Langdon were very helpful with mineral separations. This work also benefited from ongoing conversations with James Girardi, Jerome Guynn, and Scott Johnston. Comments on an early version of the manuscript by Jiba Ganguly improved the paper.

References

- Andronicos, C.L., Chardon, D.H., and Hollister, L.S., 2003, Strain partitioning in an obliquely convergent orogen, plutonism, and synorogenic collapse: Coast Mountains Batholith, British Columbia, Canada: *Tectonics*, v. 22.
- Andronicos, C.L., Hollister, L.S., Davidson, C., and Chardon, D., 1999, Kinematics and tectonic significance of transpressive structures within the Coast Plutonic Complex, British Columbia: *Journal of Structural Geology*, v. 21, p. 229-243.
- Arnold, J., Powell, R., and Sandiford, M., 2000, Amphibolites with staurolite and other aluminous minerals: calculated mineral equilibria in NCFMASH: *Journal of Metamorphic Geology*, v. 18, p. 23-40.
- Babeyko, A.Y., Sobolev, S.V., Trumbull, R.B., Oncken, O., and Lavier, L.L., 2002, Numerical models of crustal scale convection and partial melting beneath the Altiplano-Puna plateau: *Earth and Planetary Science Letters*, v. 199, p. 373-388.

- Berg, H.C., Jones, D.L., and Richter, D.H., 1972, Gravina-Nutzotin Belt - Tectonic significance of an upper Mesozoic sedimentary and volcanic sequence in southeastern Alaska: U.S. Geological Survey Professional Paper, v. 800-D, p. D1-D24.
- Berman, R.G., 1988, Internally-Consistent Thermodynamic Data for Minerals in the System Na₂O-K₂O-CaO-MgO-FeO-Fe₂O₃-Al₂O₃-SiO₂-TiO₂-H₂O-Co₂: Journal of Petrology, v. 29, p. 445-522.
- Butler, R.F., Gehrels, G.E., Baldwin, S.L., and Davidson, C., 2002, Paleomagnetism and geochronology of the Ecstall pluton in the Coast Mountains of British Columbia: Evidence for local deformation rather than large-scale transport: Journal of Geophysical Research-Solid Earth, v. 107.
- Butler, R.F., Gehrels, G.E., Hart, W., Davidson, C., and Crawford, M.L., 2006, Paleomagnetism of Late Jurassic to mid-Cretaceous plutons near Prince Rupert, British Columbia, in Haggart, J.W., Enkin, R.J. and Monger, J.W.H., eds., Paleogeography of the North American Cordillera: Evidence For and Against Large-Scale Displacements: Geological Association of Canada, Special Paper 46, p. 171-200.
- Colpron, M., Nelson, J.L., and Murphy, D.C., 2007, Northern Cordilleran terranes and their interactions through time: GSA Today, v. 17, p. 4-10.
- Cooper, A.F., and Lovering, J.F., 1970, Greenschist Amphiboles from Haast-River, New-Zealand: Contributions to Mineralogy and Petrology, v. 27, p. 11.

- Crawford, M.L., and Hollister, L.S., 1982, Contrast of Metamorphic and Structural Histories across the Work Channel Lineament, Coast Plutonic Complex, British-Columbia: *Journal of Geophysical Research*, v. 87, p. 3849-3860.
- Crawford, M.L., Hollister, L.S., and Woodsworth, G.J., 1987, Crustal deformation and regional metamorphism across a terrane boundary, Coast Plutonic Complex, British Columbia: *Tectonics*, v. 6, p. 343-361.
- Douce, A.E.P., Johnston, A.D., and Rice, J.M., 1993, Octahedral Excess Mixing Properties in Biotite - a Working Model with Applications to Geobarometry and Geothermometry: *American Mineralogist*, v. 78, p. 113-131.
- Elkins, L.T., and Grove, T.L., 1990, Ternary Feldspar Experiments and Thermodynamic Models: *American Mineralogist*, v. 75, p. 544-559.
- Faryad, S.W., and Hoinkes, G., 2006, Reaction textures in Al-rich metabasite; implication for metamorphic evolution of the eastern border of the Middle Austroalpine basement units: *Lithos*, v. 90, p. 145-157.
- Ganguly, J., Cheng, W.J., and Tirone, M., 1996, Thermodynamics of aluminosilicate garnet solid solution: New experimental data, an optimized model, and thermometric applications: *Contributions to Mineralogy and Petrology*, v. 126, p. 137-151.
- Gareau, S.A., 1991a, Geology of the Scotia-Quaal metamorphic belt, Coast Plutonic Complex, British Columbia [PhD thesis]: Ottawa, Carleton University, 390 p.
- , 1991b, The Scotia-Quaal metamorphic belt: A distinct assemblage with pre- early Late Cretaceous deformational and metamorphic history, Coast Plutonic

- Complex, British Columbia: Canadian Journal of Earth Sciences, v. 28, p. 870-880.
- Gehrels, G., Valencia, V., and Pullen, A., 2006, Detrital zircon geochronology by laser-ablation multicollector ICPMS at the Arizona Laserchron Center. In: T.O. Huff, Editor: Geochronology: Emerging Opportunities, Paleontological Society Short Course. Philadelphia, PA, p. 1-10.
- Gehrels, G.E., 2002, Detrital zircon geochronology of the Taku terrane, southeast Alaska: Canadian Journal of Earth Sciences, v. 39, p. 921-931.
- Gehrels, G.E., and Boghossian, N.D., 2000, Reconnaissance geology and U-Pb geochronology of the west flank of the Coast Mountains between Bella Coola and Prince Rupert, coastal British Columbia, in Stowell, H.H., and McClelland, W.C., eds., Tectonics of the Coast Mountains, Southeastern Alaska and British Columbia: Geological Society of America, Special Paper 343, p. 61-75.
- Gehrels, G.E., McClelland, W.C., Samson, S.D., Patchett, P.J., and Jackson, J.L., 1990, Ancient Continental-Margin Assemblage in the Northern Coast Mountains, Southeast Alaska and Northwest Canada: Geology, v. 18, p. 208-211.
- Graham, C.M., and Powell, R., 1984, A Garnet Hornblende Geothermometer - Calibration, Testing, and Application to the Pelona Schist, Southern-California: Journal of Metamorphic Geology, v. 2, p. 13-31.
- Grew, E.S., and Sandiford, M., 1985, Staurolite in a garnet-hornblende-biotite schist from the Lanterman Range, northern Victoria Land, Antarctica: Neues Jahrbuch für Mineralogie: Monatshefte, v. 9, p. 396-410.

- Hanchar, J.M., and Watson, E.B., 2003, Zircon saturation thermometry: *Zircon*, v. 53, p. 89-112.
- Himmelberg, G.R., and Brew, D.A., 2004, Thermobarometric constraints on mid-Cretaceous to Late Cretaceous metamorphic events in the western metamorphic belt of the Coast Mountains Complex near Petersburg, southeastern Alaska: U.S. Geological Survey Professional Paper, 1709-C, p. 1-18.
- Holdaway, M.J., 2000, Application of new experimental and garnet Margules data to the garnet-biotite geothermometer: *American Mineralogist*, v. 85, p. 881-892.
- Holland, T.J.B., and Powell, R., 1998, An internally consistent thermodynamic data set for phases of petrological interest: *Journal of Metamorphic Geology*, v. 16, p. 309-343.
- Hollister, L.S., 1977, The reaction forming cordierite from garnet, the Khtada Lake metamorphic complex, British Columbia: *Canadian Mineralogist*, v. 15, p. 217-229.
- , 1982, Metamorphic Evidence for Rapid (2 Mm/Yr) Uplift of a Portion of the Central-Gneiss-Complex, Coast Mountains, Bc: *Canadian Mineralogist*, v. 20, p. 319-332.
- Hollister, L.S., and Andronicos, C.L., 2006, Formation of new continental crust in Western British Columbia during transpression and transtension: *Earth and Planetary Science Letters*, v. 249, p. 29-38.
- Journey, J.M., Williams, S.P., and Wheeler, J.O., 2000, Tectonic assemblage map, Prince Rupert, British Columbia-U.S.A.: Geological Association of Canada, Open File 2948d, scale 1:1000000.

- Klepeis, K.A., Crawford, M.L., and Gehrels, G., 1998, Structural history of the crustal-scale Coast shear zone north of Portland Canal, southeast Alaska and British Columbia: *Journal of Structural Geology*, v. 20, p. 883-904.
- Kohn, M.J., and Spear, F.S., 1990, 2 New Geobarometers for Garnet Amphibolites, with Applications to Southeastern Vermont: *American Mineralogist*, v. 75, p. 89-96.
- Koziol, A.M., and Newton, R.C., 1988, Redetermination of the Anorthite Breakdown Reaction and Improvement of the Plagioclase-Garnet-Al₂SiO₅-Quartz Geobarometer: *American Mineralogist*, v. 73, p. 216-223.
- Ludwig, K.R., 2001, Isoplot/Ex, rev.2.49: Berkeley Geochronology Center, Special Publication, v. 1a.
- McClelland, W.C., Anovitz, L.M., and Gehrels, G.E., 1991, Thermobarometric Constraints on the Structural Evolution of the Coast Mountains Batholith, Central Southeastern Alaska: *Canadian Journal of Earth Sciences*, v. 28, p. 912-928.
- McClelland, W.C., Gehrels, G.E., and Saleeby, J.B., 1992a, Upper Jurassic-Lower Cretaceous Basinal Strata Along the Cordilleran Margin - Implications for the Accretionary History of the Alexander-Wrangellia-Peninsular Terrane: *Tectonics*, v. 11, p. 823-835.
- McClelland, W.C., Gehrels, G.E., Samson, S.D., and Patchett, P.J., 1992b, Structural and Geochronological Relations Along the Western Flank of the Coast Mountains Batholith - Stikine River to Cape Fanshaw, Central Southeastern Alaska: *Journal of Structural Geology*, v. 14, p. 475-489.

- Miller, C.F., McDowell, S.M., and Mapes, R.W., 2003, Hot and cold granites? Implications of zircon saturation temperatures and preservation of inheritance: *Geology*, v. 31, p. 529-532.
- Monger, J.W.H., Price, R.A., and Tempelman-Kluit, D.J., 1982, Tectonic accretion and the origin of the two major metamorphic and plutonic belts in the Canadian Cordillera: *Geology*, v. 10, p. 70-75.
- Norlander, B.H., Whitney, D.L., Teyssier, C., and Vanderhaeghe, O., 2002, Partial melting and decompression of the Thor-Odin dome, Shuswap metamorphic core complex, Canadian Cordillera: *Lithos*, v. 61, p. 103-125.
- Ouzegane, K., Bendaoud, A., Kienast, J.R., and Touret, J.L.R., 2001, Pressure-temperature-fluid evolution in Eburnean metabasites and metapelites from Tamanrasset (Hoggar, Algeria): *Journal of Geology*, v. 109, p. 247-263.
- Papike, J.J., 1987, Chemistry of the Rock-Forming Silicates - Ortho, Ring, and Single-Chain Structures: *Reviews of Geophysics*, v. 25, p. 1483-1526.
- Patchett, P.J., Gehrels, G.E., and Isachsen, C.E., 1998, Nd isotopic characteristics of metamorphic and plutonic rocks of the Coast Mountains near Prince Rupert, British Columbia: *Canadian Journal of Earth Sciences*, v. 35, p. 556-561.
- Powell, R., and Holland, T.J.B., 1988, An Internally Consistent Dataset with Uncertainties and Correlations.3. Applications to Geobarometry, Worked Examples and a Computer-Program: *Journal of Metamorphic Geology*, v. 6, p. 173-204.

- Rubin, C.M., Saleeby, J.B., Cowan, D.S., Brandon, M.T., and McGroder, M.F., 1990, Regionally Extensive Midcretaceous West-Vergent Thrust System in the Northwestern Cordillera - Implications for Continent-Margin Tectonism: *Geology*, v. 18, p. 276-280.
- Rusmore, M.E., Gehrels, G., and Woodsworth, G.J., 2001, Southern continuation of the Coast shear zone and Paleocene strain partitioning in British Columbia-southeast Alaska: *Geological Society of America Bulletin*, v. 113, p. 961-975.
- Rusmore, M.E., Woodsworth, G.J., and Gehrels, G.E., 2005, Two-stage exhumation of midcrustal arc rocks, Coast Mountains, British Columbia: *Tectonics*, v. 24, p. -.
- Rusmore, M.E., Woodsworth, G.J., Gehrels, G.E., and Fjeld, K., 2006, Evolution of the western metamorphic belt in the Coast Mountains arc, Bella Bella, British Columbia (Lat 52-53): Preliminary Results: *Geological Society of America Abstracts with Programs*, v. 38, p. 268.
- Selverstone, J., Spear, F.S., Franz, G., and Morteani, G., 1984, High-Pressure Metamorphism in the Sw Tauern Window, Austria - P-T Paths from Hornblende-Kyanite-Staurolite Schists: *Journal of Petrology*, v. 25, p. 501-531.
- Spear, F.S., 1995, Metamorphic phase equilibria and pressure-temperature-time paths: Mineralogical Society of America, Washington, D.C., Mongraph 1, 799 p.
- Spear, F.S., and Cheney, J.T., 1989, A Petrogenetic Grid for Pelitic Schists in the System $\text{SiO}_2\text{-Al}_2\text{O}_3\text{-FeO-MgO-K}_2\text{O-H}_2\text{O}$: *Contributions to Mineralogy and Petrology*, v. 101, p. 149-164.

- Stacey, J.S., and Kramers, J.D., 1975, Approximation of Terrestrial Lead Isotope Evolution by a 2-Stage Model: *Earth and Planetary Science Letters*, v. 26, p. 207-221.
- Stowell, H., and Crawford, M.L., 2000, Metamorphic history of the Coast Mountains orogen, western British Columbia and southeastern Alaska, in Stowell, H.H. and McClelland, W.C., eds., *Tectonics of the Coast Mountains, Southeastern Alaska and British Columbia: Geological Society of America, Special Paper 343*, p. 257-283.
- Stowell, H.H., Taylor, D.L., Tinkham, D.L., Goldberg, S.A., and Ouderkirk, K.A., 2001, Contact metamorphic P-T-t paths from Sm-Nd garnet ages, phase equilibria modelling and thermobarometry: Garnet Ledge, south-eastern Alaska, USA: *Journal of Metamorphic Geology*, v. 19, p. 645-660.
- Sutter, J.F., and Crawford, M.L., 1985, Timing of metamorphism and uplift in the vicinity of Prince Rupert, British Columbia and Ketchikan, Alaska: *Geological Society of America Abstracts with Programs*, v. 17, p. 411.
- Thompson, A.B., and England, P.C., 1984, Pressure Temperature Time Paths of Regional Metamorphism. 2. Their Inference and Interpretation Using Mineral Assemblages in Metamorphic Rocks: *Journal of Petrology*, v. 25, p. 929-955.
- van der Heyden, P., 1992, A Middle Jurassic to Early Tertiary Andean-Sierran arc model for the Coast belt of British Columbia: *Tectonics*, v. 11, p. 82-97.

Figures

Figure 1. Location of study area. Modified from Rusmore et al. (2005) and Butler et al. (2006).

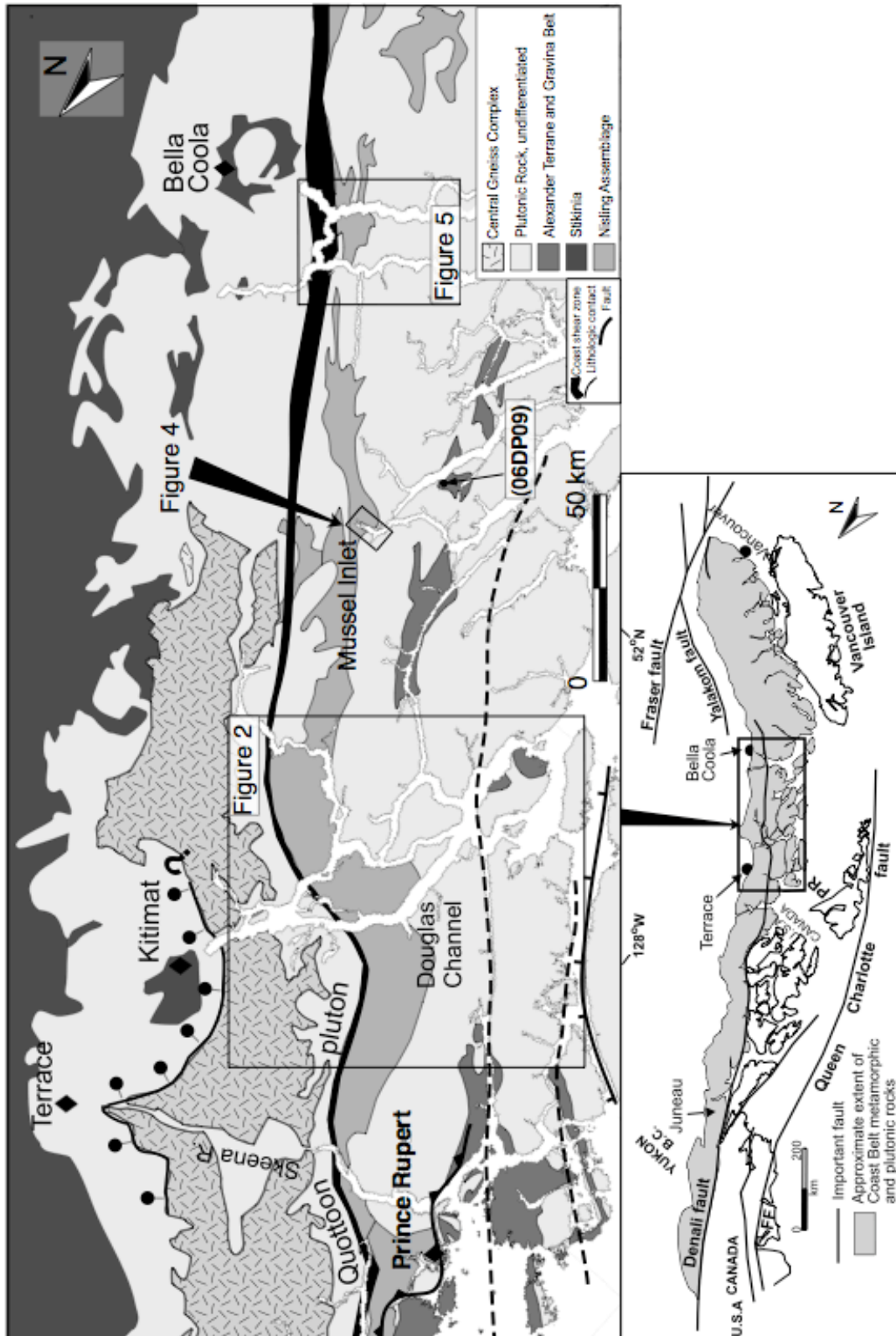


Figure 2. General geologic map of Douglas Channel and Prince Rupert regions showing sample localities from this study. Modified from Rusmore et al. (2005), Gehrels and Boghossian (2000), Butler et al. (2006), and Hollister (1982).

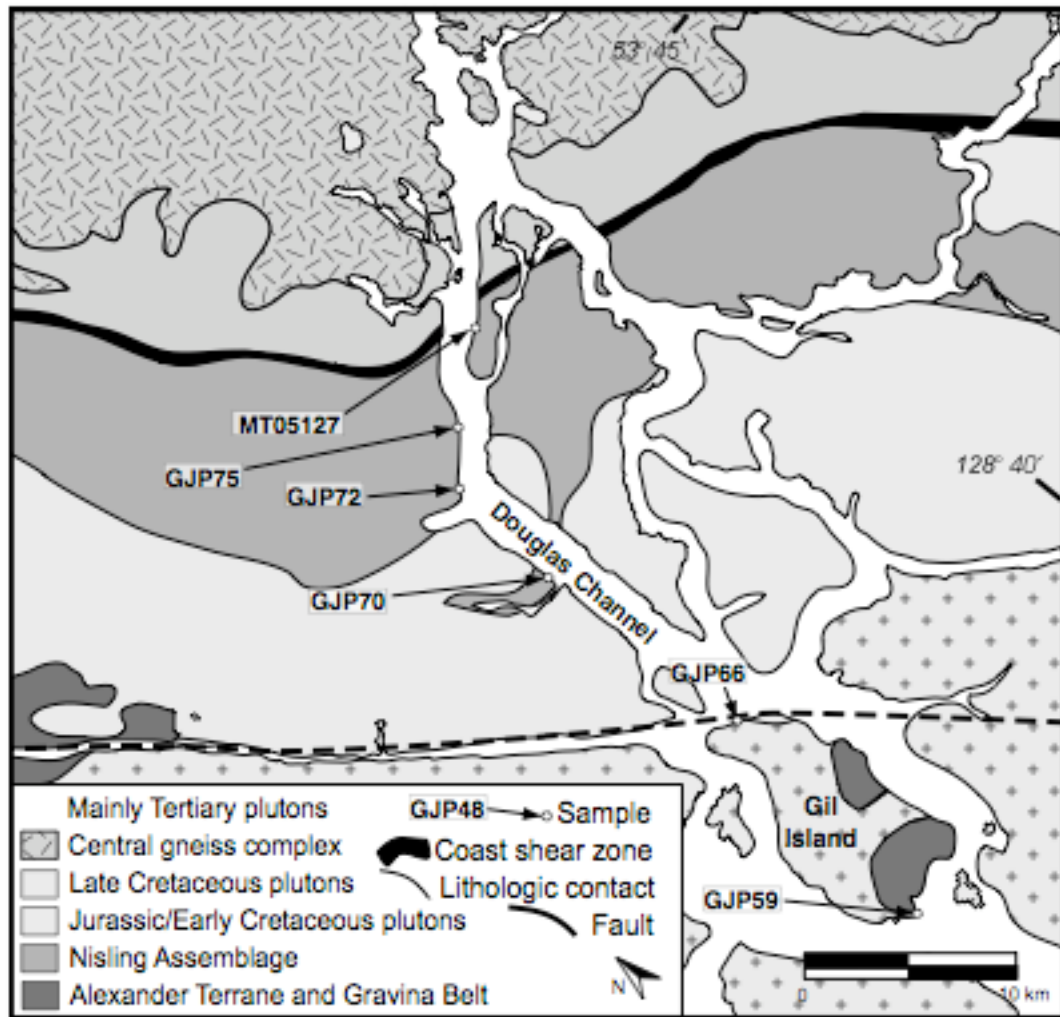


Figure 3. Photomicrographs of phase relationships used to constrain P-T-t paths of metasedimentary rocks. More detailed descriptions are given in text. a) Sample GJP75 includes polygonal garnet hypidoblasts with inclusions defining an earlier crenulation cleavage; b) Samples GJP48, GJP49, and MT05100 contain crystallographically oriented sillimanite pseudomorphs, possibly of kyanite; c) Biotite in sample GJP48 is commonly intergrown with sillimanite and rarely is rimmed by it; d) Garnet-amphibolite sample 06DP07 contains garnet with idioblastic staurolite inclusions; e) Sample GJP28 contains amphibole with tschermakitic cores and cummingtonitic rims.

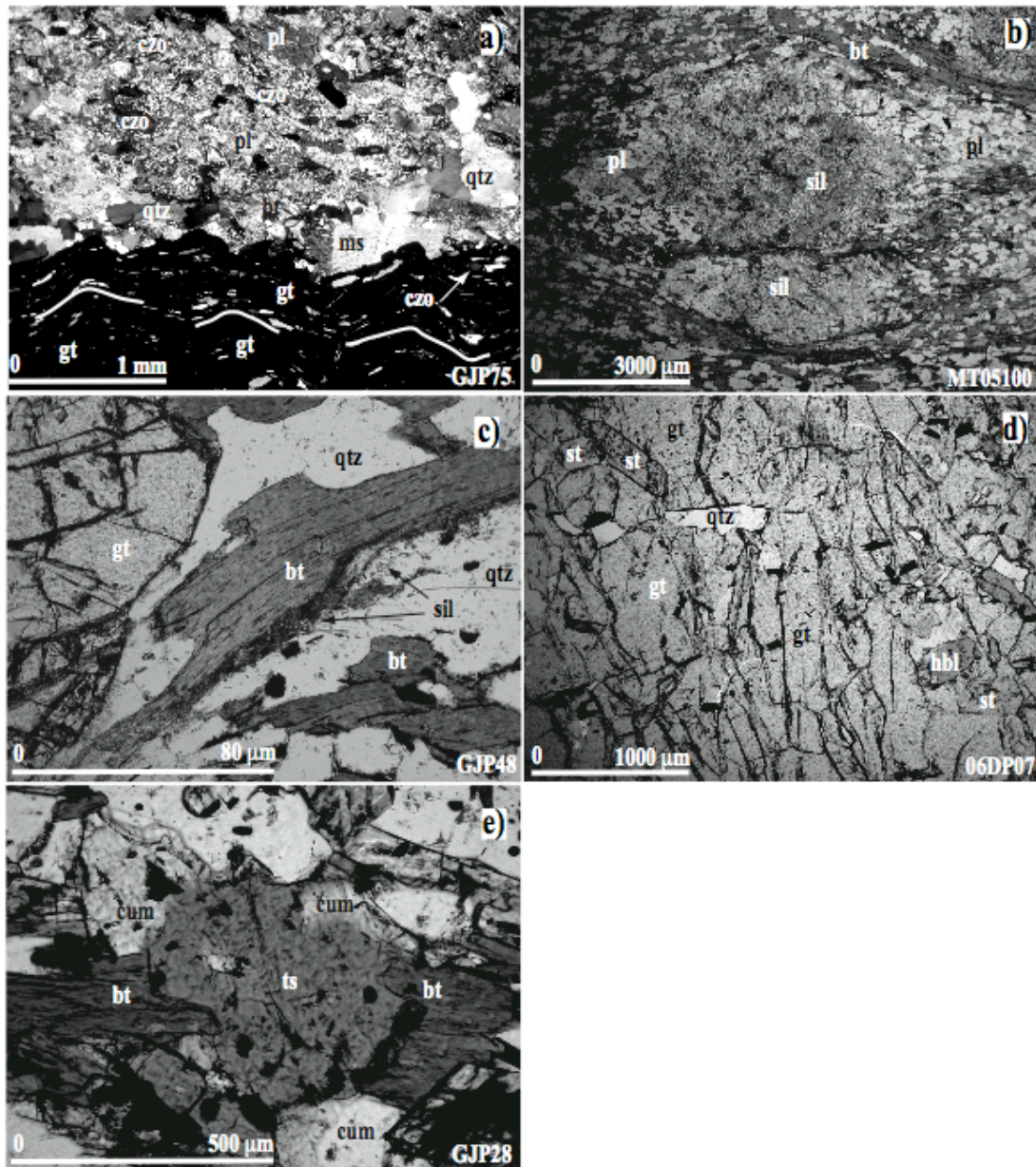


Figure 4. General geologic map of Mussel Inlet showing sample locations and U-Pb zircon results from this study and relevant unpublished U-Pb zircon results (G. Gehrels, pers. comm., 2006). Modified from Baer et al. (1972).

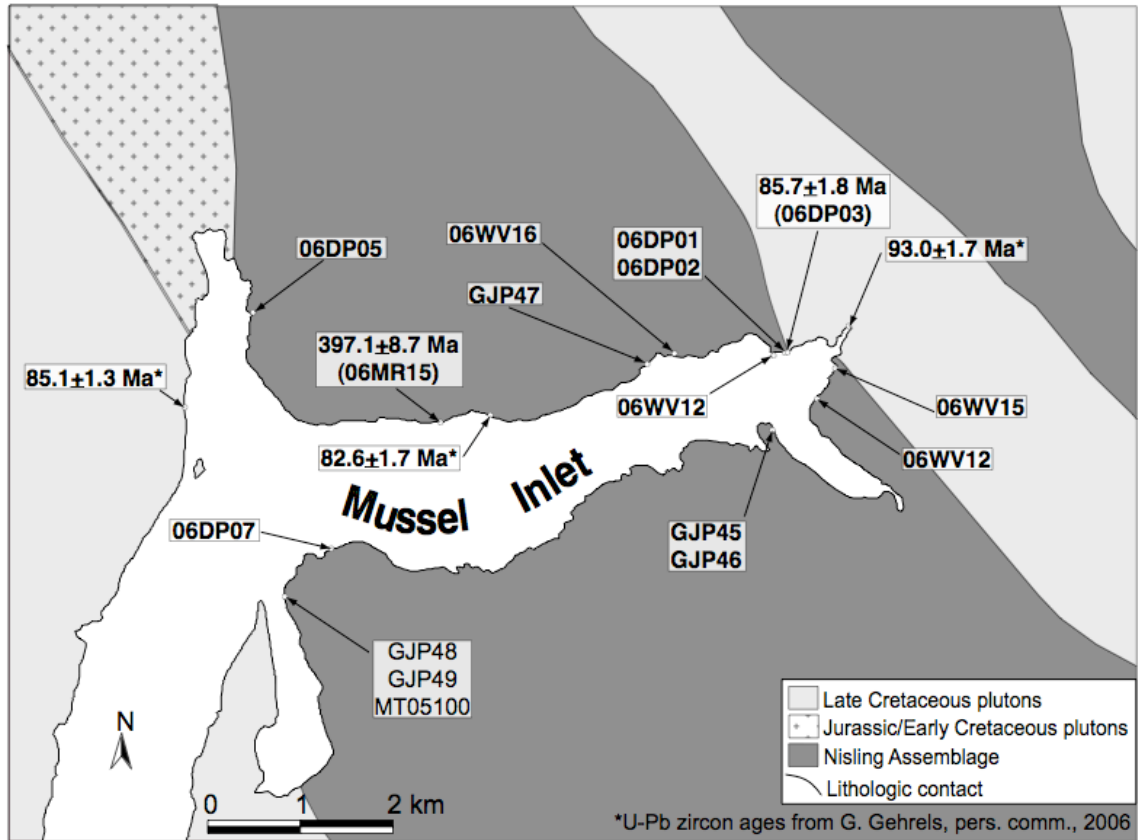


Figure 5. Simplified geologic map of Dean and Burke Channels, west of Bella Coola. Modified from Gehrels and Boghossian (2000) and Rusmore et al. (2005).

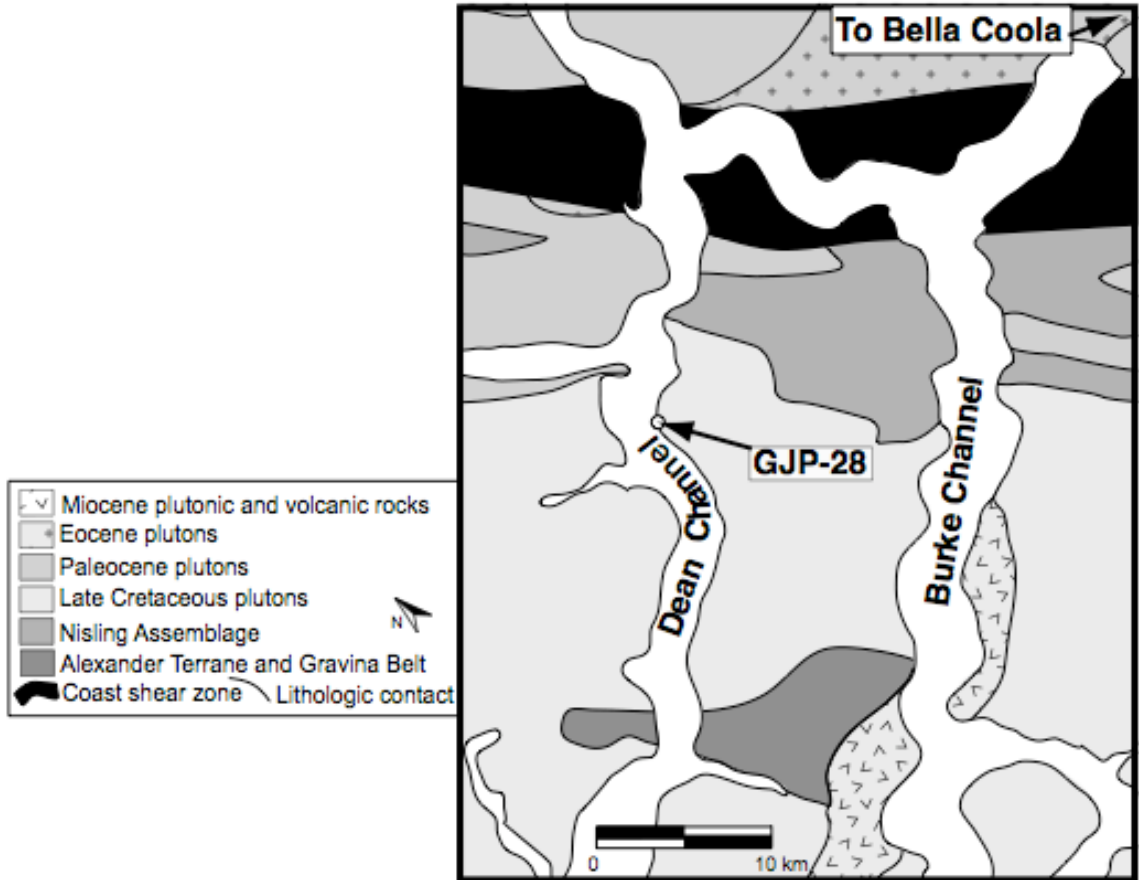


Figure 6. U-Pb concordia and average age plots (Ludwig, 2001) for three zircon samples. Error ellipses represent 1σ errors and only reflect measurement uncertainties. Mean: uncertainty from weighted mean calculation, including measurement errors. Age: final uncertainty of age, including both systematic and measurement errors. a) Sample 06DP03; b) Sample 06DP09; c) Sample 06MR15.

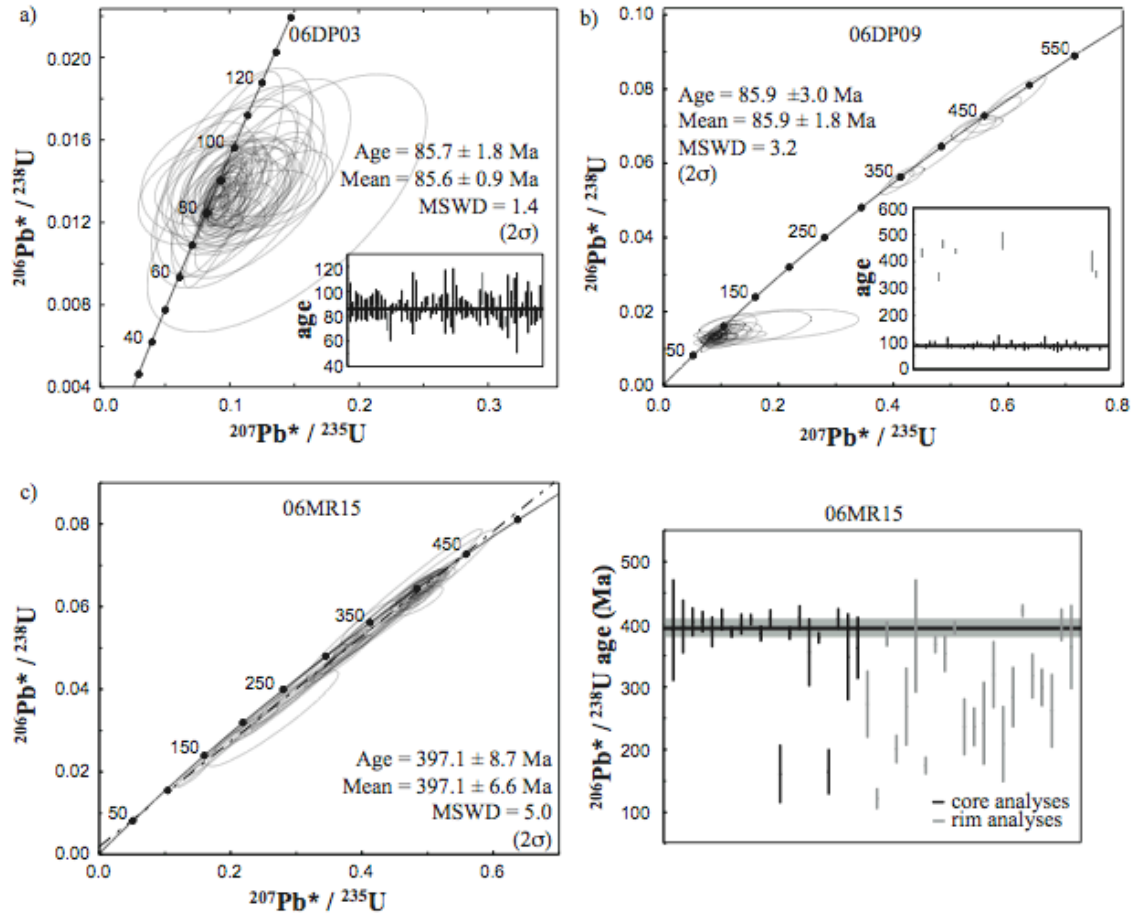


Figure 7. Representative diffusion zoning in garnet.

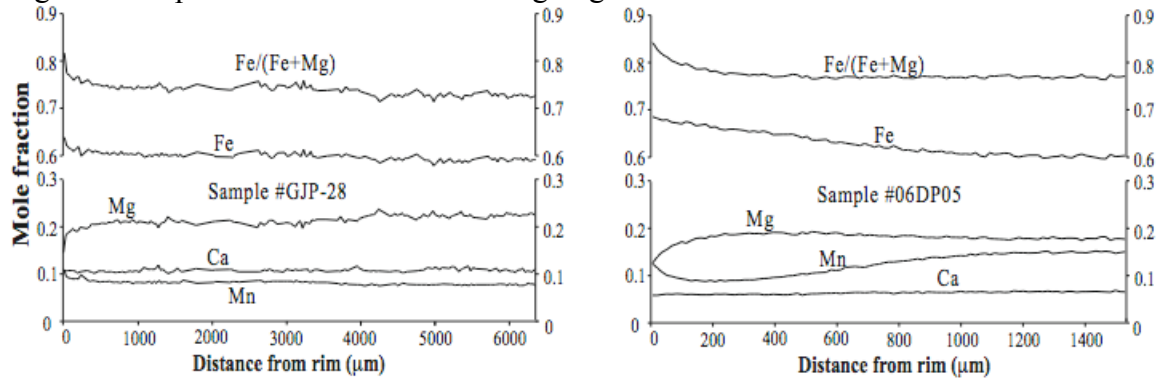
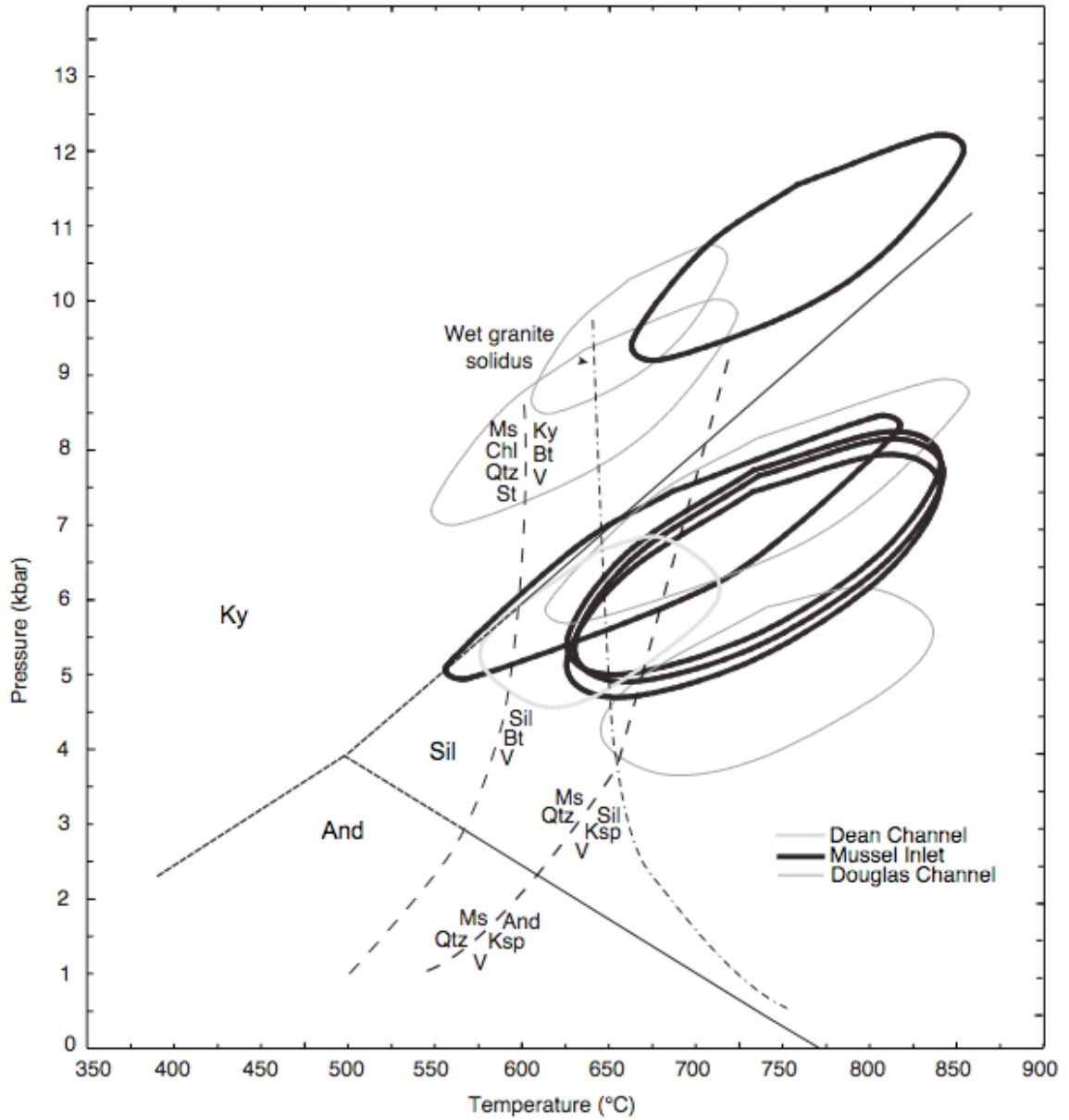


Figure 8. P-T plots of THERMOCALC (Powell and Holland, 1988) results and corresponding error ellipses from this study.



Tables

Table 1. Mineral assemblages of metamorphic rocks from the current study. “x”-stable, “[x]”-relict and metastable, “r”-interpreted as retrograde. Mineral abbreviations are: chl-chlorite, ms-muscovite, bt-biotite, grt-garnet, st-staurolite, crd-cordierite, and-andalusite, sil-sillimanite, ky-kyanite, amp-amphibole, czo-clinozoisite, ep-epidote, cpx-clinopyroxene, opx-orthopyroxene, qtz-quartz, kfs-K-feldspar, and pl-plagioclase.

Sample	Metamorphic minerals																
	chl	ms	bt	grt	st	crd	and	sil	ky	amp	czo	ep	cpx	opx	qtz	kfs	pl
GJP28	-	-	x	x	-	-	-	-	-	x	-	-	-	-	-	x	x
GJP45	-	-	x	x	-	-	-	-	-	-	-	-	-	-	x	x	x
GJP46	r	-	x	x	-	-	-	-	-	-	-	-	-	-	x	x	x
GJP47	r	-	x	x	-	-	-	-	-	x	-	-	-	-	x	x	x
GJP48	-	r	x	x	-	-	-	x	-	-	-	-	-	-	x	x	x
GJP49	-	r	x	x	-	-	-	x	-	-	-	-	-	-	x	x	x
GJP59	r	[x]	x	x	-	-	-	-	-	x	-	-	-	-	x	-	x
GJP66	r	-	x	x	-	-	-	-	-	x	-	r	-	-	x	-	x
GJP70	[x]	r	x	x	-	-	-	-	-	-	-	-	-	-	x	x	x
GJP72	r	x	x	x	-	-	-	-	-	x	-	-	-	-	x	-	x
GJP75	x	x	[x]	[x]	-	-	-	-	-	-	x	-	-	-	x	-	x
MT05100	-	[x]	x	x	-	-	-	x	-	-	-	-	-	-	x	x	x
MT05127	r	x	x	x	[x]	-	-	-	x	-	-	-	-	-	x	-	x
06DP01	-	-	x	x	-	-	-	-	-	x	-	-	-	-	x	x	x
06DP02	-	-	x	x	-	-	-	-	-	-	-	-	-	-	x	x	x
06DP05	-	[x]	x	x	-	-	-	x	-	-	-	-	-	-	x	-	x
06DP07	[x]	[x]	x	x	[x]	-	-	-	-	x	-	-	-	-	x	x	x
06WV12	-	-	x	x	-	-	-	-	-	x	-	-	-	-	x	x	x
06WV14	r	-	x	x	-	-	-	-	-	x	-	r	-	-	x	x	x
06WV15	r	-	x	x	-	-	-	-	-	x	-	-	-	-	x	x	x
06WV16	-	[x]	x	x	-	-	-	x	-	-	-	-	-	-	x	-	x

Table 2. Results from individual U-Pb zircon analyses by LA-MC-ICPMS. Given errors are at the 1 σ level and reflect only measurement uncertainties. U concentration and U/Th have uncertainties of ~25%. Decay constants: $^{235}\text{U}=9.8485\times 10^{-10}$, $^{238}\text{U}=1.55125\times 10^{-10}$, $^{238}\text{U}/^{235}\text{U}=137.88$. Isotope ratios are corrected for Pb/U fractionation by comparison with standard zircon with an age of 564 ± 4 Ma. Initial Pb composition determined from Stacey and Kramers (1975), with uncertainties of 1.0 for $^{206}\text{Pb}/^{204}\text{Pb}$ and 0.3 for $^{207}\text{Pb}/^{204}\text{Pb}$.

Sample	Isotopic ratios							Apparent ages (Ma)								
	U (ppm)	$^{206}\text{Pb}/^{204}\text{Pb}$	U/Th	$^{207}\text{Pb}^*/^{235}\text{U}$ (%)	\pm	$^{206}\text{Pb}^*/^{238}\text{U}$ (%)	\pm	Error Corr.	$^{206}\text{Pb}^*/^{238}\text{U}$ (Ma)	\pm	$^{207}\text{Pb}^*/^{235}\text{U}$ (Ma)	\pm	Best age (Ma)	\pm		
06DP03 (52.918357°N, 128.039602°W)																
grain																
1c	77	360	2.3	0.19937	16.1	0.01425	8.8	0.55	91.2	7.9	184.6	27.1	1651.0	250.5	91.2	7.9
2c	90	996	1.7	0.12913	11.9	0.01340	3.5	0.29	85.8	3.0	123.3	13.9	925.0	235.3	85.8	3.0
3c	81	1142	2.4	0.11018	14.8	0.01372	7.0	0.47	87.8	6.1	106.1	15.0	539.2	286.9	87.8	6.1
4c	91	1185	2.1	0.11227	11.7	0.01374	5.9	0.50	88.0	5.2	108.0	12.0	576.2	220.1	88.0	5.2
5c	105	1675	4.2	0.10805	9.4	0.01353	5.8	0.61	86.7	5.0	104.2	9.3	525.9	163.6	86.7	5.0
6c	72	1650	3.7	0.11107	11.6	0.01336	4.9	0.42	85.5	4.1	106.9	11.7	614.7	227.2	85.5	4.1
7c	97	1389	2.4	0.10901	14.3	0.01327	5.4	0.38	85.0	4.6	105.1	14.3	588.4	288.7	85.0	4.6
8c	72	1337	2.5	0.10916	10.7	0.01381	4.5	0.42	88.4	4.0	105.2	10.7	504.4	214.5	88.4	4.0
9c	67	1068	2.2	0.11212	13.2	0.01380	5.6	0.43	88.3	5.0	107.9	13.6	565.1	261.8	88.3	5.0
10c	69	1062	2.1	0.13047	11.1	0.01399	7.0	0.63	89.5	6.2	124.5	13.0	857.9	177.8	89.5	6.2
11c	70	864	2.7	0.12991	9.2	0.01384	6.7	0.73	88.6	5.9	124.0	10.7	871.5	130.3	88.6	5.9
12c	144	782	2.2	0.14312	10.5	0.01363	5.5	0.53	87.3	4.8	135.8	13.3	1098.9	178.0	87.3	4.8
13c	2017	16666	520.2	0.08949	4.8	0.01339	4.6	0.96	85.7	4.0	87.0	4.0	122.5	30.3	85.7	4.0
14c	442	2828	34.0	0.09296	15.1	0.01184	5.0	0.33	75.9	3.8	90.3	13.0	489.8	315.8	75.9	3.8
15c	234	1526	16.3	0.08926	11.3	0.01164	9.8	0.86	74.6	7.2	86.8	9.4	436.7	126.9	74.6	7.2
16c	502	7311	34.7	0.09238	3.5	0.01349	2.5	0.71	86.4	2.1	89.7	3.0	179.0	57.9	86.4	2.1
17c	617	7040	30.9	0.09387	2.5	0.01357	1.7	0.68	86.9	1.5	91.1	2.2	203.2	42.0	86.9	1.5
18c	501	5600	19.3	0.10285	2.9	0.01403	2.0	0.70	89.8	1.8	99.4	2.8	336.2	47.5	89.8	1.8
19c	1428	10947	3.4	0.09522	13.9	0.01379	7.3	0.52	88.3	6.4	92.4	12.3	199.1	276.7	88.3	6.4
20c	534	4904	18.5	0.09950	2.6	0.01361	2.0	0.75	87.2	1.7	96.3	2.4	329.3	38.8	87.2	1.7
21r	523	3990	31.4	0.09845	7.7	0.01334	4.6	0.61	85.4	3.9	95.3	7.0	352.0	137.8	85.4	3.9
22r	555	6260	63.6	0.08610	4.6	0.01242	2.8	0.62	79.6	2.2	83.9	3.7	207.8	83.3	79.6	2.2
23c	53	1045	2.5	0.12412	22.8	0.01414	14.0	0.61	90.5	12.5	118.8	25.6	730.8	384.7	90.5	12.5
24c	47	866	2.4	0.10303	28.5	0.01443	9.0	0.32	92.3	8.3	99.6	27.0	276.7	628.6	92.3	8.3
25r	516	8415	72.1	0.09046	3.9	0.01275	2.0	0.52	81.7	1.6	87.9	3.3	260.8	77.2	81.7	1.6
26r	398	3543	15.4	0.09612	5.3	0.01362	2.5	0.48	87.2	2.2	93.2	4.8	248.9	108.3	87.2	2.2
27r	393	3746	16.1	0.10513	4.8	0.01394	3.5	0.74	89.2	3.1	101.5	4.6	399.9	72.4	89.2	3.1
28r	690	7017	64.0	0.10151	3.0	0.01441	2.1	0.69	92.3	1.9	98.2	2.8	244.3	50.1	92.3	1.9
29r	505	4044	55.5	0.09303	3.2	0.01272	2.0	0.62	81.5	1.6	90.3	2.7	331.3	56.4	81.5	1.6
30r	189	2396	5.9	0.11332	5.7	0.01408	4.6	0.81	90.1	4.1	109.0	5.8	543.7	72.1	90.1	4.1
31r	545	5768	4.1	0.09519	5.2	0.01339	2.5	0.48	85.8	2.1	92.3	4.6	265.3	104.1	85.8	2.1

Table 2. (Cont'd).

Sample	Isotopic ratios							Apparent ages (Ma)								
	U (ppm)	$^{206}\text{Pb}/^{204}\text{Pb}$	U/Th	$^{207}\text{Pb}^*/^{235}\text{U}$ (%)	\pm	$^{206}\text{Pb}^*/^{238}\text{U}$ (%)	\pm	Error Corr.	$^{206}\text{Pb}^*/^{238}\text{U}$ (Ma)	\pm	$^{207}\text{Pb}^*/^{235}\text{U}$ (Ma)	\pm	$^{206}\text{Pb}^*/^{207}\text{Pb}^*$ (Ma)	\pm	Best age (Ma)	\pm
32r	707	5435	41.8	0.10305	3.3	0.01428	2.3	0.69	91.4	2.1	99.6	3.2	299.6	55.0	91.4	2.1
33c	269	3550	4.4	0.10026	9.0	0.01355	6.4	0.71	86.7	5.5	97.0	8.3	357.4	143.5	86.7	5.5
34c	189	2916	4.3	0.09821	18.0	0.01434	14.1	0.79	91.8	12.9	95.1	16.3	179.5	259.4	91.8	12.9
35c	104	1591	3.3	0.08586	20.8	0.01379	5.7	0.28	88.3	5.0	83.6	16.7	-47.8	491.2	88.3	5.0
36r	181	1027	3.9	0.10612	12.0	0.01237	5.2	0.43	79.3	4.1	102.4	11.7	681.7	232.3	79.3	4.1
37c	67	1614	2.6	0.10356	24.0	0.01443	14.3	0.60	92.4	13.1	100.1	22.9	287.3	443.8	92.4	13.1
38c	60	1165	2.9	0.08580	16.4	0.01456	6.5	0.40	93.2	6.0	83.6	13.2	-182.4	378.8	93.2	6.0
39r	205	2501	6.1	0.09522	7.8	0.01383	3.4	0.44	88.6	3.0	92.4	6.9	191.4	164.1	88.6	3.0
40r	324	2890	24.0	0.10140	9.5	0.01358	5.4	0.57	87.0	4.7	98.1	8.9	376.8	177.0	87.0	4.7
41c	154	2190	3.2	0.08930	11.0	0.01339	4.3	0.39	85.8	3.6	86.9	9.2	116.8	240.3	85.8	3.6
42r	457	3626	7.7	0.09943	7.6	0.01339	3.7	0.49	85.7	3.2	96.2	7.0	364.9	149.0	85.7	3.2
43r	557	3759	12.4	0.09329	5.0	0.01339	2.3	0.45	85.8	1.9	90.6	4.4	218.9	103.6	85.8	1.9
45r	900	5818	1.9	0.08806	3.9	0.01300	2.5	0.63	83.2	2.0	85.7	3.2	154.4	71.9	83.2	2.0
46r	549	3266	5.0	0.08602	6.5	0.01254	2.5	0.39	80.3	2.0	83.8	5.2	183.7	138.8	80.3	2.0
47c	88	1554	3.9	0.09859	19.7	0.01358	8.5	0.43	86.9	7.3	95.5	17.9	314.3	406.5	86.9	7.3
48r	152	4502	5.4	0.12962	10.8	0.01597	6.3	0.59	102.1	6.4	123.8	12.6	562.2	190.2	102.1	6.4
49r	96	1241	4.2	0.09684	14.7	0.01393	6.0	0.41	89.2	5.3	93.9	13.2	215.1	312.7	89.2	5.3
50c	60	1249	4.1	0.07734	25.4	0.01336	7.4	0.29	85.5	6.3	75.6	18.5	-226.4	620.8	85.5	6.3
51c	202	1280	1.1	0.08856	9.8	0.01419	5.1	0.52	90.8	4.6	86.2	8.1	-41.4	204.4	90.8	4.6
52c	330	6968	30.3	0.09963	5.6	0.01365	4.5	0.81	87.4	3.9	96.4	5.1	326.4	74.8	87.4	3.9
53r	193	2742	8.2	0.09893	5.5	0.01286	3.3	0.59	82.4	2.7	95.8	5.0	444.1	98.7	82.4	2.7
54c	71	1280	2.7	0.10976	17.3	0.01311	7.8	0.45	84.0	6.5	105.7	17.4	629.6	334.6	84.0	6.5
55r	380	4207	9.4	0.09206	8.9	0.01200	5.1	0.57	76.9	3.9	89.4	7.6	438.3	162.6	76.9	3.9
56r	365	2952	55.8	0.09288	7.6	0.01186	2.7	0.36	76.0	2.1	90.2	6.5	484.2	155.9	76.0	2.1
57r	63	886	3.0	0.10631	25.7	0.01372	14.6	0.57	87.8	12.8	102.6	25.0	460.4	471.8	87.8	12.8
58r	415	5940	10.0	0.10013	7.6	0.01404	5.9	0.79	89.9	5.3	96.9	7.0	273.6	106.9	89.9	5.3
59r	80	1123	5.9	0.10343	19.3	0.01444	10.0	0.52	92.4	9.1	99.9	18.3	283.2	379.3	92.4	9.1
60r	83	608	4.0	0.14422	30.6	0.01293	19.7	0.64	82.8	16.2	136.8	39.2	1218.5	467.2	82.8	16.2
61c	364	7269	7.4	0.08689	5.7	0.01297	2.6	0.45	83.1	2.1	84.6	4.6	127.8	118.7	83.1	2.1
62r	275	3614	3.9	0.09463	7.3	0.01338	3.2	0.44	85.7	2.7	91.8	6.4	254.6	150.0	85.7	2.7
63c	80	1623	2.9	0.11229	14.4	0.01402	5.7	0.40	89.7	5.1	108.1	14.7	533.6	289.9	89.7	5.1
64r	228	2947	68.9	0.11310	14.5	0.01365	12.0	0.83	87.4	10.4	108.8	14.9	607.5	174.5	87.4	10.4
65c	97	1791	3.0	0.11123	23.5	0.01348	7.8	0.33	86.3	6.7	107.1	23.9	597.5	484.5	86.3	6.7

Table 2. (Cont'd).

Sample	Isotopic ratios							Apparent ages (Ma)								
	U (ppm)	$^{206}\text{Pb}/^{207}\text{Pb}$	U/Th	$^{207}\text{Pb}^*/^{235}\text{U}$ (%)	\pm	$^{206}\text{Pb}^*/^{238}\text{U}$ (%)	\pm	Error	$^{206}\text{Pb}^*/^{238}\text{U}$ (Ma)	\pm	$^{207}\text{Pb}^*/^{235}\text{U}$ (Ma)	\pm	$^{206}\text{Pb}^*/^{207}\text{Pb}^*$ (Ma)	\pm	Best age (Ma)	\pm
66r	280	2984	1.8	0.09640	8.3	0.01265	4.3	0.52	81.0	3.5	93.4	7.4	423.7	159.3	81.0	3.5
67r	284	3046	2.5	0.09609	5.6	0.01275	3.5	0.63	81.7	2.9	93.2	5.0	398.0	98.5	81.7	2.9
68r	136	2587	10.3	0.12402	12.7	0.01433	7.3	0.58	91.7	6.7	118.7	14.2	700.9	221.6	91.7	6.7
06DP09 (52.705822 ⁿ N, 128.215670 ^w W)																
grain																
1c	347	3163	1.1	0.09579	5.5	0.01394	3.5	0.63	89.2	3.1	92.9	4.9	187.7	99.8	89.2	3.1
2c	646	24500	2.3	0.53990	2.9	0.06944	2.0	0.69	432.8	8.4	438.4	10.4	467.6	47.2	432.8	8.4
3c	166	1495	2.2	0.09154	6.9	0.01333	4.7	0.69	85.4	4.0	88.9	5.8	186.1	116.2	85.4	4.0
4c	126	1534	2.6	0.11082	10.5	0.01518	4.2	0.40	97.1	4.1	106.7	10.7	326.9	218.8	97.1	4.1
5c	145	1871	2.2	0.11700	6.1	0.01529	3.3	0.55	97.8	3.2	112.3	6.5	433.1	113.5	97.8	3.2
6c	1256	42502	1.2	0.40778	2.9	0.05485	2.5	0.85	344.2	8.2	347.3	8.5	367.6	34.3	344.2	8.2
7c	218	9501	1.3	0.59199	2.2	0.07489	1.7	0.77	465.5	7.5	472.1	8.2	504.4	30.4	465.5	7.5
8c	704	2447	1.0	0.11056	19.3	0.01549	10.2	0.53	99.1	10.0	106.5	19.5	275.8	376.9	99.1	10.0
9c	564	2453	0.5	0.08964	9.6	0.01339	3.5	0.37	85.7	3.0	87.2	8.0	126.5	210.0	85.7	3.0
11c	136	4393	1.7	0.55764	2.4	0.07048	1.2	0.51	439.0	5.1	450.0	8.6	506.3	44.8	439.0	5.1
12c	302	3275	2.4	0.09310	3.7	0.01320	2.8	0.76	84.5	2.4	90.4	3.2	247.6	56.1	84.5	2.4
14c	208	1709	1.5	0.09330	7.8	0.01288	3.4	0.43	82.5	2.8	90.6	6.8	308.2	161.6	82.5	2.8
15c	490	4845	2.8	0.15745	2.5	0.02240	1.6	0.63	142.8	2.2	148.5	3.4	239.6	44.5	142.8	2.2
16c	238	3027	1.8	0.09550	6.1	0.01392	3.1	0.51	89.1	2.8	92.6	5.4	182.8	122.0	89.1	2.8
17c	115	1097	1.2	0.10552	15.9	0.01331	6.8	0.43	85.2	5.7	101.9	15.4	511.3	318.2	85.2	5.7
18c	618	4924	5.4	0.10454	4.8	0.01498	4.2	0.87	95.9	4.0	101.0	4.6	222.7	55.0	95.9	4.0
19c	771	5015	1.5	0.09869	4.1	0.01447	2.5	0.62	92.6	2.3	95.6	3.7	170.2	75.0	92.6	2.3
20c	329	2733	2.0	0.09149	5.1	0.01355	2.5	0.50	86.8	2.2	88.9	4.3	146.3	103.4	86.8	2.2
22c	443	3358	2.5	0.08919	5.3	0.01319	3.4	0.65	84.5	2.9	86.7	4.4	149.4	93.9	84.5	2.9
23c	53	627	2.6	0.11860	17.8	0.01374	9.7	0.54	88.0	8.4	113.8	19.2	694.0	320.4	88.0	8.4
24c	58	715	1.7	0.20147	28.1	0.01655	10.1	0.36	105.8	10.6	186.4	48.0	1388.9	513.0	105.8	10.6
25c	150	6556	1.3	0.60815	3.9	0.07695	3.5	0.91	477.9	16.2	482.4	14.9	503.9	35.1	477.9	16.2
26c	170	1504	2.1	0.10632	8.5	0.01309	4.7	0.55	83.9	3.9	102.6	8.3	563.0	155.4	83.9	3.9
27c	281	2075	1.2	0.10901	11.9	0.01489	7.4	0.63	95.3	7.0	105.1	11.8	332.1	210.5	95.3	7.0
29r	2468	4267	2.4	0.09552	14.9	0.01274	5.0	0.34	81.6	4.1	92.6	13.2	386.1	316.5	81.6	4.1
30r	2589	15854	2.4	0.09294	2.8	0.01428	1.7	0.59	91.4	1.5	90.2	2.4	60.1	54.1	91.4	1.5
31r	412	1123	2.8	0.11331	14.8	0.01320	8.9	0.60	84.5	7.4	109.0	15.3	683.6	254.9	84.5	7.4
32r	255	2412	1.0	0.09356	14.1	0.01289	4.6	0.32	82.6	3.8	90.8	12.3	313.0	305.8	82.6	3.8

Table 2. (Cont'd).

Sample	Isotopic ratios							Apparent ages (Ma)						
	U (ppm)	$^{206}\text{Pb}/^{203}\text{Pb}$	U/Th	$^{207}\text{Pb}^*/^{235}\text{U}$ (%)	\pm	$^{206}\text{Pb}^*/^{238}\text{U}$ (%)	\pm Error	$^{206}\text{Pb}^*/^{238}\text{U}$ (Ma)	\pm	$^{207}\text{Pb}^*/^{235}\text{U}$ (Ma)	\pm	$^{206}\text{Pb}^*/^{207}\text{Pb}^*$ (Ma)	\pm Best age	\pm
33r	522	1715	4.1	0.09978	11.9	0.01349	2.7 0.23	86.4	2.4	96.6	11.0	355.5	262.5	86.4 2.4
34r	352	1061	3.6	0.11574	22.5	0.01388	3.5 0.16	88.9	3.1	111.2	23.7	620.7	484.1	88.9 3.1
35r	264	5387	3.0	0.09457	7.9	0.01403	5.1 0.64	89.8	4.5	91.7	6.9	141.8	142.9	89.8 4.5
36r	360	514	2.6	0.16990	20.8	0.01573	11.6 0.56	100.6	11.6	159.3	30.7	1154.8	345.8	100.6 11.6
37r	499	5239	2.5	0.08238	6.3	0.01275	3.8 0.60	81.7	3.1	80.4	4.9	42.9	121.3	81.7 3.1
38r	472	1573	2.6	0.09258	10.6	0.01281	7.7 0.72	82.1	6.3	89.9	9.1	303.2	166.8	82.1 6.3
39r	967	2950	9.2	0.09314	12.4	0.01288	11.7 0.94	82.5	9.6	90.4	10.7	305.3	92.4	82.5 9.6
40r	416	2309	3.7	0.08892	5.9	0.01262	3.8 0.63	80.9	3.0	86.5	4.9	244.7	106.1	80.9 3.0
41r	282	3626	3.0	0.10187	10.0	0.01513	6.7 0.67	96.8	6.4	98.5	9.4	139.4	174.1	96.8 6.4
42r	1699	5995	2.5	0.08059	6.1	0.01238	3.4 0.56	79.3	2.7	78.7	4.6	60.6	121.0	79.3 2.7
43r	116	1192	2.1	0.11166	14.9	0.01425	7.0 0.47	91.2	6.3	107.5	15.2	485.2	292.1	91.2 6.3
44r	316	704	8.0	0.09069	8.8	0.01219	4.4 0.50	78.1	3.4	88.1	7.4	369.1	171.2	78.1 3.4
45r	583	1963	2.5	0.08937	4.2	0.01254	2.5 0.60	80.3	2.0	86.9	3.5	271.6	78.1	80.3 2.0
46r	550	1011	2.2	0.09125	7.3	0.01174	5.1 0.70	75.2	3.8	88.7	6.2	467.9	116.0	75.2 3.8
48r	1321	43848	5.5	0.49039	5.1	0.08428	4.9 0.95	401.6	19.0	405.2	17.1	425.5	34.4	401.6 19.0
49r	1383	30555	2.0	0.42230	2.9	0.05636	2.1 0.70	353.4	7.1	357.7	8.8	385.3	46.7	353.4 7.1
50r	1290	1064	3.2	0.07572	12.7	0.01187	3.4 0.27	76.1	2.6	74.1	9.1	11.9	295.1	76.1 2.6
51r	1810	4189	5.8	0.09090	4.3	0.01319	1.7 0.39	84.5	1.4	88.3	3.7	193.8	93.0	84.5 1.4
52c	223	3572	2.4	0.45852	9.4	0.05915	8.1 0.86	370.5	29.2	383.2	30.1	460.9	106.7	370.5 29.2
53r	204	535	5.3	0.34161	26.0	0.03960	17.4 0.67	250.3	42.8	298.4	67.3	693.7	414.5	250.3 42.8
54r	76	445	4.1	0.26224	18.6	0.02899	13.7 0.74	184.2	25.0	236.5	39.3	794.2	264.5	184.2 25.0
06MR15 (52.909921°N, 128.096269°W)														
grain														
1c	460	11772	0.7	0.47611	10.7	0.06246	10.5 0.98	390.6	39.8	395.4	35.2	423.7	48.0	390.6 39.8
2c	721	25702	1.6	0.48343	5.5	0.06339	5.4 0.98	396.2	20.7	400.4	18.2	424.7	23.1	396.2 20.7
3c	501	14426	1.1	0.48799	3.1	0.06465	2.8 0.90	403.8	10.9	403.5	10.3	401.8	30.1	403.8 10.9
4c	873	31666	1.1	0.49243	2.2	0.06471	2.0 0.89	404.2	7.8	406.6	7.5	419.8	22.5	404.2 7.8
5c	518	21711	1.8	0.47549	3.3	0.06203	3.1 0.94	387.9	11.5	395.0	10.7	436.3	24.3	387.9 11.5
6c	597	25437	1.8	0.50470	2.3	0.06526	2.0 0.88	407.5	8.0	414.9	7.8	456.0	23.8	407.5 8.0
7c	1236	38673	1.4	0.46781	1.4	0.06196	1.0 0.71	387.5	3.8	389.7	4.6	402.5	22.5	387.5 3.8
8c	617	23355	1.4	0.48240	2.2	0.06409	2.0 0.89	400.5	7.7	399.7	7.3	395.5	22.8	400.5 7.7
9c	898	26579	1.1	0.49156	1.4	0.06524	1.0 0.71	407.4	4.0	406.0	4.8	397.6	22.5	407.4 4.0
10c	590	22689	1.8	0.47986	2.0	0.06157	1.5 0.75	385.2	5.7	398.0	6.7	473.1	29.9	385.2 5.7

Table 2. (Cont'd).

Sample	Isotopic ratios							Apparent ages (Ma)								
	U (ppm)	$^{206}\text{Pb}/^{204}\text{Pb}$	U/Th	$^{207}\text{Pb}^*/^{235}\text{U}$ (%)	\pm	$^{206}\text{Pb}^*/^{238}\text{U}$ (%)	\pm	Error	$^{206}\text{Pb}^*/^{238}\text{U}$ (Ma)	\pm	$^{207}\text{Pb}^*/^{235}\text{U}$ (Ma)	\pm	$^{206}\text{Pb}^*/^{207}\text{Pb}^*$ (Ma)	\pm	Best age (Ma)	\pm
11c	601	22392	1.2	0.50454	1.9	0.06556	1.7	0.86	409.4	6.6	414.8	6.6	444.9	22.4	409.4	6.6
12c	1150	15254	7.7	0.18375	14.3	0.02530	14.2	0.99	161.1	22.6	171.3	22.6	315.0	42.8	161.1	22.6
13c	784	32909	2.1	0.46935	1.6	0.06169	1.2	0.78	385.9	4.7	390.7	5.2	419.5	22.5	385.9	4.7
14c	903	30606	0.9	0.49925	2.5	0.06580	2.3	0.92	410.8	9.1	411.2	8.4	413.3	22.5	410.8	9.1
16c	1142	25478	1.2	0.43250	7.7	0.05665	7.6	0.99	355.2	26.4	365.0	23.6	427.4	22.9	355.2	26.4
17c	1052	27542	1.7	0.46550	1.9	0.06046	1.1	0.57	378.4	4.0	388.1	6.1	446.1	34.8	378.4	4.0
18c	1176	18842	5.3	0.18728	10.8	0.02587	10.7	0.99	164.7	17.4	174.3	17.3	307.1	32.6	164.7	17.4
19c	690	22135	1.2	0.49967	2.2	0.06549	1.9	0.87	408.9	7.7	411.5	7.5	425.8	24.7	408.9	7.7
20c	438	12509	2.1	0.41889	10.2	0.05547	10.0	0.98	348.0	34.0	355.3	30.7	402.7	44.0	348.0	34.0
21r	716	20323	1.2	0.43168	7.0	0.05783	6.9	0.98	362.4	24.2	364.4	21.5	376.6	33.0	362.4	24.2
22r	736	19763	2.0	0.31805	9.8	0.04319	9.7	0.99	272.6	26.0	280.4	24.1	346.1	28.4	272.6	26.0
23r	692	5658	10.6	0.13909	6.9	0.01907	6.3	0.90	121.8	7.5	132.2	8.6	324.5	67.3	121.8	7.5
24r	1143	31537	0.5	0.48476	3.2	0.06146	2.5	0.76	384.5	9.2	401.3	10.8	499.3	46.4	384.5	9.2
25r	879	14651	2.6	0.23887	5.7	0.03167	5.3	0.93	201.0	10.5	217.5	11.2	400.2	46.0	201.0	10.5
26r	1048	23815	1.2	0.32189	11.6	0.04256	11.6	1.00	268.7	30.4	283.4	28.7	406.4	22.8	268.7	30.4
27r	807	24346	1.1	0.44884	12.2	0.06096	12.0	0.99	381.4	44.5	376.5	38.4	345.9	47.5	381.4	44.5
28r	1261	25787	3.3	0.19510	4.2	0.02746	3.7	0.87	174.6	6.4	181.0	7.0	264.8	47.9	174.6	6.4
29r	676	19844	1.1	0.44646	2.2	0.05864	1.7	0.78	367.4	6.1	374.8	6.9	421.0	30.7	367.4	6.1
31r	622	19618	1.3	0.41614	4.7	0.05627	4.0	0.86	352.9	13.8	353.3	13.9	356.0	53.7	352.9	13.8
32c	469	18905	1.1	0.48672	1.9	0.06309	1.2	0.66	394.4	4.7	402.7	6.2	450.3	31.0	394.4	4.7
33r	756	11073	2.3	0.28744	9.6	0.03738	9.5	0.98	236.6	22.0	256.5	21.8	443.2	37.5	236.6	22.0
34r	497	9604	2.7	0.28223	6.7	0.03735	6.3	0.95	236.4	14.7	252.4	14.9	404.2	46.3	236.4	14.7
36r	988	43601	2.7	0.28249	13.8	0.03825	13.7	0.99	242.0	32.4	252.6	30.8	353.0	41.9	242.0	32.4
37r	443	11971	1.7	0.39331	8.4	0.05085	8.3	0.99	319.8	26.0	336.8	24.1	456.1	23.0	319.8	26.0
38r	866	1923	2.5	0.26456	15.4	0.03294	14.4	0.94	208.9	29.6	238.3	32.7	539.3	117.9	208.9	29.6
40r	561	18177	1.7	0.33795	8.7	0.04503	8.5	0.98	283.9	23.5	295.6	22.2	389.0	42.0	283.9	23.5
41c	858	30849	0.7	0.52272	1.6	0.06759	1.1	0.67	421.6	4.3	427.0	5.5	456.0	26.0	421.6	4.3
43r	937	17507	1.2	0.38951	5.6	0.05046	5.5	0.98	317.3	17.2	334.0	16.0	451.8	22.6	317.3	17.2
44r	883	13777	1.2	0.36852	5.2	0.04749	4.9	0.95	299.1	14.4	318.6	14.1	463.5	34.5	299.1	14.4
45r	831	15373	1.9	0.31905	11.2	0.04149	11.2	1.00	262.0	28.7	281.2	27.6	443.5	24.5	262.0	28.7
46c	512	26149	1.7	0.48646	3.6	0.06389	3.2	0.87	399.2	12.2	402.5	12.0	421.2	39.3	399.2	12.2
47r	944	29866	1.2	0.44443	9.4	0.05807	9.3	0.99	363.9	33.0	373.4	29.5	432.8	32.6	363.9	33.0

Table 3. Representative electron microprobe analyses for minerals used in thermobarometric calculations. “Spot” refers to analysis locations: “c”-core, “r”-rim (for grt, inside retrograde diffusion profile), “m”-matrix grain away from grt. “na”-not analyzed.

Sample min spot	GJP28 Grt c	GJP28 Bt mc	GJP28 Pl mr	GJP28 Amp mc	GJP47 Grt r	GJP47 Bt mc	GJP47 Pl mr	GJP47 Amp mc	GJP48 Grt r	GJP48 Bt mc	GJP48 Pl mr	GJP49 Grt r
Wt%												
SiO ₂	38.21	36.26	54.98	42.27	37.78	35.39	57.14	42.13	37.16	35.01	60.23	36.74
TiO ₂	0.02	1.44	0.12	0.87	0.04	2.81	0.00	1.51	0.05	3.12	0.00	0.02
Al ₂ O ₃	21.79	18.18	27.84	15.15	21.01	16.94	26.68	13.22	42.63	19.43	25.19	20.47
Cr ₂ O ₃	0.04	0.02	0.01	0.04	0.00	0.01	0.03	0.02	0.01	0.02	0.00	0.00
FeO	26.98	14.67	0.34	14.09	24.92	20.35	0.04	18.16	34.04	18.57	0.00	24.69
MnO	3.54	0.09	0.00	0.38	2.33	0.08	0.02	0.22	1.91	0.09	0.05	15.23
MgO	5.78	14.73	0.00	10.61	2.46	9.34	0.00	7.92	4.17	9.00	0.00	1.69
CaO	3.66	0.02	9.23	10.39	10.65	0.04	8.15	11.40	1.34	0.00	6.15	1.18
Na ₂ O	0.00	0.61	6.67	1.76	0.01	0.21	6.92	1.33	0.00	0.29	8.18	0.06
K ₂ O	na	8.05	0.00	0.29	na	9.29	0.27	1.29	na	8.96	0.08	na
Total	100.01	94.08	99.19	95.85	99.21	94.45	99.24	97.19	100.00	94.49	99.88	100.87

Sample min spot	GJP49 Bt mc	GJP49 Pl mr	GJP59 Grt r	GJP59 Bt mc	GJP59 Pl mr	GJP70 Grt r	GJP70 Bt mc	GJP70 Ms mc	GJP70 Pl mr	GJP72 Grt r	GJP72 Bt mc	GJP72 Ms mc
Wt%												
SiO ₂	35.00	60.74	38.36	35.76	48.51	36.74	34.85	47.95	65.43	36.95	33.94	45.48
TiO ₂	2.77	0.00	0.02	2.01	0.04	0.02	2.83	1.03	0.00	0.00	1.81	0.13
Al ₂ O ₃	19.76	25.29	21.48	18.99	33.37	20.47	16.28	33.76	21.80	21.23	18.66	37.30
Cr ₂ O ₃	0.04	0.03	0.05	0.05	0.00	0.00	0.00	0.00	0.03	0.03	0.03	0.00
FeO	19.45	0.01	29.95	15.55	0.05	24.69	24.73	4.49	0.07	30.10	22.41	2.05
MnO	0.07	0.01	2.58	0.08	0.00	15.23	0.47	0.03	0.00	5.04	0.08	0.01
MgO	8.34	0.00	6.07	12.09	0.00	1.69	6.82	0.99	0.00	1.31	7.83	0.64
CaO	0.00	6.31	1.84	0.02	15.84	1.18	0.00	0.00	2.20	6.10	0.00	0.00
Na ₂ O	0.30	8.10	0.04	0.20	2.67	0.06	0.14	0.34	10.74	0.01	0.22	1.01
K ₂ O	8.83	0.09	na	9.35	0.02	na	9.66	9.93	0.15	na	9.05	9.96
Total	94.56	100.59	100.38	94.11	100.49	100.08	95.79	98.52	100.42	100.78	94.04	96.58

Sample min spot	GJP72 Pl mr	GJP72 Amp mc	MT05100 Grt r	MT05100 Bt mc	MT05100 Pl mr	MT05127 Grt c	MT05127 Bt mc	MT05127 Ms mc	MT05127 Pl mr	06DP05 Grt r	06DP05 Bt mc	06DP05 Pl mr
Wt%												
SiO ₂	55.71	37.92	37.69	35.67	59.67	37.45	36.01	45.83	62.36	37.66	36.03	57.83
TiO ₂	0.00	0.24	0.00	3.11	0.00	0.04	1.99	0.79	0.00	0.00	2.26	0.00
Al ₂ O ₃	28.16	20.35	21.13	19.82	25.50	21.31	19.53	37.38	23.76	21.46	19.30	27.19
Cr ₂ O ₃	0.00	0.00	0.02	0.00	0.00	0.00	0.04	0.02	0.00	0.02	0.01	0.05
FeO	0.05	20.67	33.95	19.26	0.02	32.48	16.63	0.91	0.00	30.14	17.22	0.10
MnO	0.00	0.23	2.07	0.04	0.03	1.57	0.03	0.00	0.00	4.11	0.12	0.00
MgO	0.00	3.99	3.96	8.57	0.00	4.39	11.44	0.76	0.00	4.81	10.98	0.00
CaO	9.64	11.05	1.52	0.00	6.64	2.66	0.00	0.00	4.36	2.16	0.00	8.58
Na ₂ O	6.33	1.28	0.03	0.23	7.95	0.00	0.47	1.43	9.39	0.04	0.16	7.01
K ₂ O	0.04	0.49	na	8.91	0.07	na	8.77	8.89	0.09	na	9.06	0.10
Total	99.95	96.24	100.38	95.63	99.87	99.91	94.92	96.01	99.97	100.41	95.16	100.86

Table 4. Comparison of geothermobarometric results from this study. ¹GASP barometry and GarB thermometry from formulations by Ganguly and Cheng, 1996; ²THERMOCALC (Powell and Holland, 1988) results with error correlation factor (cor.); ³GAP barometry of Kohn and Spear, 1990; ⁴GA thermometry from Graham and Powell, 1984

Sample	GASP barom ¹		GarB thermom ¹		THERMOCALC ²					GAP barom ³		GA thermom ⁴	
	P (kbar)	±	T (°C)	±	P (kbar)	±	T (°C)	±	cor.	P (kbar)	±	T (°C)	±
GJP-28	na		695	50	5.7	0.9	645	54	0.519	3.7	0.5	600	50
GJP-47	na		750	50	10.7	1.2	760	76	0.828	7.2	0.5	720	50
GJP-48	5.4	0.5	740	50	6.5	1.3	738	85	0.717	na		na	
GJP-49	5.9	0.5	775	50	6.3	1.3	735	86	0.720	na		na	
GJP-59	na		745	50	4.9	1.0	742	76	0.605	na		na	
GJP-70	na		780	50	7.3	1.3	737	97	0.855	na		na	
GJP-72	na		600	50	8.5	1.2	637	70	0.831	4.9	0.5	610	50
MT05-100	6.1	0.5	765	50	6.6	1.3	735	86	0.732	na		na	
MT05-127	8.4	0.5	675	50	9.6	0.9	663	45	0.801	na		na	
06DP05	7.0	0.5	755	50	6.7	1.4	689	104	0.903	na		na	